THE UNIVERSITY OF CALGARY

Small Antenna Radiation-Efficiency Measurement Methods

by

Jiangzuo Chu

A THESIS

SUBMITTED TO THE FACULTY OF GRADUATE STUDIES

IN PARTIAL FULFILLMENT OF THE REQUIREMENTS FOR THE

DEGREE OF MASTER OF SCIENCE

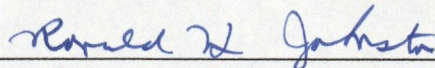DEPARTMENT OF ELECTRICAL AND COMPUTER ENGINEERING
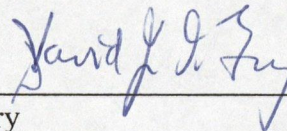
CALGARY, ALBERTA

September, 2003

UNIVERSITY OF CALGARY

FACULTY OF GRADUATE STUDIES

The undersigned certify that they have read, and recommend to the Faculty of Graduate Studies for acceptance, a thesis entitled "Small antenna radiation-efficiency measurement methods" submitted by Jiangzuo Chu in partial fulfillment of the requirements of the degree of Master of Science.

_____
Supervisor, Dr. R. H. Johnston
Department of Electrical and Computer Engineering

_____
Dr. M.Okoniewski
Department of Electrical and Computer Engineering

_____
Dr. D. Fry
Department of Physics and Astronomy

_____
Sept 12, 2003
Date

ii

Abstract

It is known that the accurate measurement of antenna radiation efficiency can be a difficult task. There are various methods of measuring the efficiency. However, some of the methods have a substantial amount of error and involve unverifiable assumptions. In this thesis, an improved method of determining antenna efficiency is described in detail. Also, large number of measurement results on various antennas are presented.

Acknowledgements

This thesis would not have happened without the help of many people. I am most grateful to my supervisor, Dr. Johnston for his guidance, assistance and patient instruction. I also thank Dr. Okoniewski for his teaching ENEL575 which gives me necessary and important background for many works in this thesis. Particular thanks go to my friends in the ICT Building, the University of Calgary.

Finally, my wholehearted gratitude is to my parents, Heng Chu and Huizhen Xiang, for their endless support regardless the distance of 10000km living away from me.

Table of Contents

List of Figures

List of Symbols and Acronyms

Γ reflection coefficient

AUT   antenna under test

FDTD   finite-difference time-domain

IF   intermediate frequency

LO   local oscillator

MATLAB   a computer language that provides a flexible environment for technical computing and simulating

PCS   personal communication system

RF   radio frequency

VNA   vector network analyzer

Chapter 1

Introduction

The antenna is an essential component in any radio system. It provides a means for radiating or receiving radio waves which may contain information. One of humankind's greatest natural resources is the electromagnetic spectrum and free space electromagnetic wave propagation and the antenna is essential in interfacing with this resource. In all cases of using this resource, antennas must be used. For example, mobile communications involving aircraft, spacecraft, ships or land vehicles require antennas. Wireless personal communication system (PCS) such as cellular phones and pagers are very popular today and antennas are always required.

1.1 Antenna definition

The official IEEE definition [1] of an antenna follows this concept: "That part of a transmitting or receiving system that is designed to radiate or receive electromagnetic waves." An antenna is a structure associated with the region of transition between a guided wave and a free-space wave. Antennas are treated as transmitting or receiving as appropriate for the particular situation. In the receiving mode, antennas act to collect incoming waves and direct them to a common feed point where a transmission line (or structure) is attached.

1.2 Types of Antennas

Antennas can be divided into four basic types by their performance as a function of frequency [1].

• Electrically small antennas: The extent of antenna structure is much less than a wavelength λ. They are simple in structure and their properties are not sensitive to construction details. They often suffer very low directivity, low radiation efficiency, and often low input resistance.

Examples:

$\ll \lambda$ $\ll \lambda$
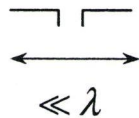
very short dipole   small loop

• Resonant antennas: The antenna operates well at a single or selected narrow frequency bands.

Examples:

$\sim \frac{\lambda}{2}$ $\sim \frac{\lambda}{2}$
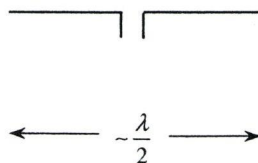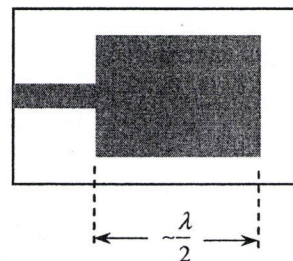
half-wave diploe   microstrip patch antenna

• Broadband antennas: The pattern, gain , and impedance remain acceptable and are nearly constant over a wide frequency range, and are characterized by an active region with a circumference of one wavelength or an extent of a half-wavelength, which relocates on the antenna as the frequency changes.

Examples:
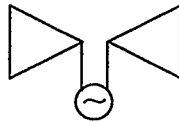
the wide-band bowtie antenna

• Aperture antennas: Have a physical aperture (opening) through which plane EM waves flow. Typically, they have very high gain and moderate bandwidth.

Examples:
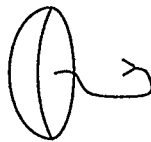
high gain reflector

1.3 Background of antenna measurements

Many antennas, with very complex structural configurations and excitation methods, can not be investigated analytically. Although many computer software packages based on special analytical methods (such as Finite-Difference Time-Domain), allow numerical

simulation, there are still a fair number of antennas that have not been analyzed mathematically. In addition, experimental results are often needed to validate theoretical data. Most of the basic methodology for measuring the characteristics of antennas was developed before and during World War II. The basic methods for the measurement of antenna far field patterns, antenna polarization, antenna input impedance, gain, directivity and efficiency were developed during this period in conjunction with the design of novel radiating structures, which were needed in the rapidly expanding telecommunication and radar technologies.

1.4 Background of antenna radiation efficiency measurements

Antenna radiation efficiency, defined as the ratio of radiated power to input power, is an important antenna parameter, especially in small antennas. It can have a great effect on the overall system performance and yet it may not always receive the attention it deserves. For example, a RF engineer must frequently make critical trade offs in receiver design in order to improve sensitivity by mere fractions of a dB, but poor antenna efficiency can easily cause a degradation of several dB. For example, if an antenna has a radiation efficiency of less than 50 percent, which corresponds to power loss of more than 3 dB, then the transmitter power loss will greatly degrade the handset's battery life and in cellular systems, it would affect the ability of the handset to obtain service in marginal areas.

Many efficiency measurement techniques, such as the Wheeler cap, directivity/gain and radiometric methods, were developed. Those measurements can suffer from quite low accuracy, require some specialized laboratory equipment, and/or rely on certain assumptions.

In this thesis, a new method of determining the radiation efficiency is described which removes assumptions of the traditional Wheeler cap method. Three kinds of measurement apparatuses, a rectangular waveguide, a precision low-loss rectangular waveguide and a cubic cavity, are developed and utilized to take efficiency measurements on various antennas. The thesis treats a high-efficiency antenna that may be regarded as a reference antenna for efficiency measurements and reference loss antennas with 3 and 6dB losses. Measurement data is presented also for monopoles and patch antennas. The measurement results indicate that the new method of antenna efficiency measurement exhibits high accuracy. In addition, good agreement of measuring results is achieved in these three measurement apparatus. However, the cubic cavity provides a more convenient measurement and can be used over a wider frequency range.

Chapter 2

Antenna Basics

2.1 Antenna Parameters

2.1.1 Radiation Patterns

An antenna radiation pattern or antenna pattern is defined as "a mathematical function or a graphical representation of the radiation properties of the antenna as a function of space coordinates" [2]. In most cases, the radiation pattern is determined in the far-field region since most practical applications are remote transmission and reception of electromagnetic wave energy. In practice, the three-dimensional pattern is measured and recorded in a series of two-dimensional patterns. However, for most practical applications, a few plots of the pattern as a function of θ for some particular values of ϕ and vice versa give most of the useful and needed information. Figure 2.1 is a typical radiation pattern of a high gain antenna.
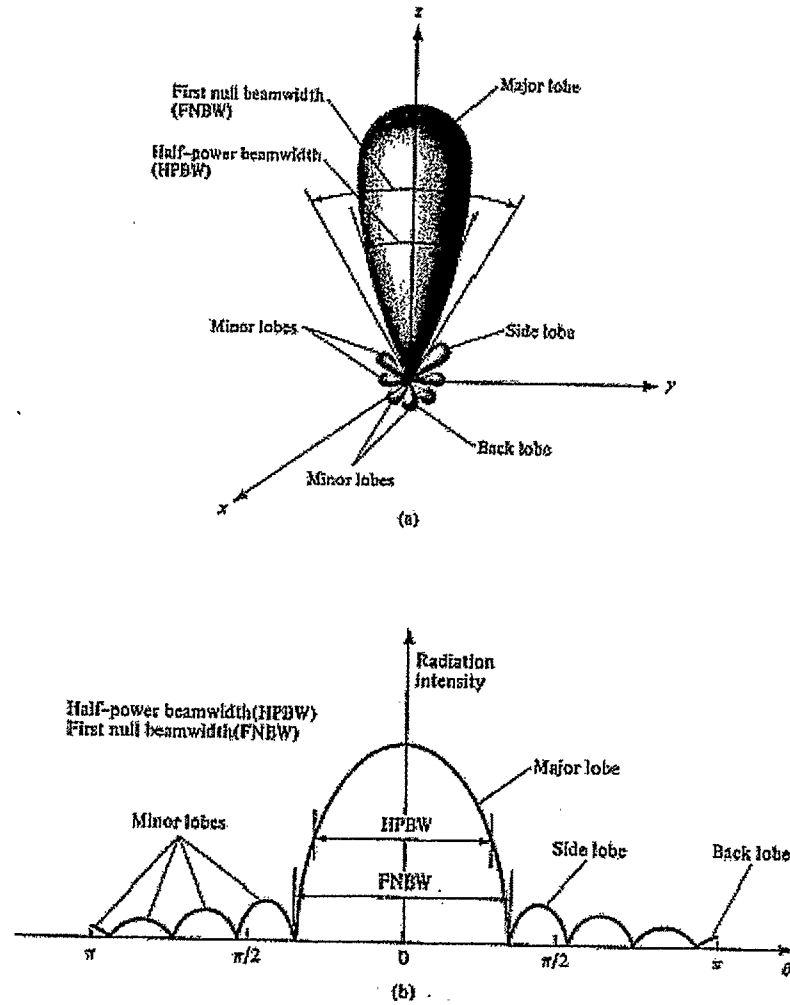
Figure 2.1 Antenna radiation pattern

The main lobe (main beam) is the lobe containing the direction of maximum radiation intensity. There is also usually a series of lobes smaller than the main lobe. Any lobe other than the main lobe is called a minor lobe. Minor lobes usually represent radiation in undesired directions, and they should normally be minimized.

Another meaningful parameter is the half-power beamwidth, HPBW. It is the angular separation of the points where the main beam of the power pattern equals one-half. Hence:

$$HPBW = \left| \theta_{Hpleft} - \theta_{Hpright} \right|, \tag{2-1}$$

where θ_{Hpleft} and $\theta_{Hpright}$ are points to the "left" and "right" of the main beam maximum for which the power pattern has the value of one-half. See Figure 2.1.

2.1.2 Directivity and Gain

One important feature of an antenna is how well it concentrates energy in one direction in preference to radiation in other directions. This characteristic of an antenna is called Directivity (D). It is given by the ratio of the maximum radiation intensity to the average radiation intensity. The average radiation intensity can be defined as the total power radiated by the antenna divided by 4π. For an isotropic source, the radiation intensity can be written as:

$$U_0 = \frac{P_{rad}}{4\pi}. \tag{2-2}$$

The directivity of a non-isotropic source is equal to the ratio of its radiation intensity in a given direction over that of an isotropic source. Using (2-2), it can be written as:

$$D = \frac{U}{U_0} = \frac{4\pi U}{P_{rad}}. \tag{2-3}$$

If the direction is not specified, it is implied that the direction of maximum radiation intensity (maximum directivity) can be expressed as:

$$D_{\max} = D_0 = \frac{U_{\max}}{U_0} = \frac{4\pi U_{\max}}{P_{rad}}, \qquad (2\text{-}4)$$

where: D = directivity (dimensionless),

         D_0 = maximum directivity (dimensionless),

         U = radiation intensity (W/unit solid angle),

         $U_{\max}$ = maximum radiation intensity (W/unit solid angle),

         U_0 = radiation intensity of isotropic source (W/unit solid angle),

         P_{rad} = total radiated power (W).

The directivity of an isotropic source is unity since its power is radiated equally in all directions. For all other sources, the maximum directivity will always be greater than unity.

Antenna gain is used to quantify not only the directive properties, but also how efficiently the antenna transforms net input power to radiated power. The directivity is a measure that describes only the directional properties of the antenna, and it is therefore controlled only by the pattern. Hence, antenna efficiency may be combined with directivity to obtain antenna gain:

$$G_{\max} = \frac{4\pi U_{\max}}{P_{rad}} \cdot \frac{P_{rad}}{P_{in}}, \qquad (2\text{-}5)$$

where P_{in} is power delivered in the antenna (input power).

2.1.3 Antenna Impedance and Radiation Resistance

The input impedance of an antenna is the impedance presented by the antenna at its terminals. The input impedance will be affected by other antennas or objects that are

nearby. Assuming the antenna is isolated, the input impedance has a constant value and is composed of a real and imaginary part:

$$Z_A = R_A + jX_A.$$ (2-6)

The input resistance R_A represents dissipation and consists of two parts. One is the power that leaves the antenna and never returns (i.e. radiation resistance). The other is ohmic loss associated with heating on the antenna structure. For electrically small antennas, ohmic losses are often significant compared with the radiation resistance. The input reactance X_A represents power stored in the near field of the antenna.

The average power delivered to an antenna P_{in} is

$$P_{in} = \frac{1}{2} R_A |I_A|^2,$$ (2-7)

where I_A is the peak current at the input terminals. Separating the delivered power into radiative and ohmic losses by $P_{in} = P_{rad} + P_{loss}$ gives:

$$\frac{1}{2} R_A |I_A|^2 = \frac{1}{2} R_r |I_A|^2 + \frac{1}{2} R_{loss} |I_A|^2,$$ (2-8)

where we define the radiation resistance R_r of an antenna referred to the input port as

$$R_r = \frac{2P_{rad}}{|I_A|^2}.$$ (2-9)

From (2-8), it is easy to get:

$$R_A = R_r + R_{loss}.$$ (2-10)

In some small antennas, R_r and R_{loss} can be measured at the antenna terminal, but in many antennas, R_r, R_{loss} and X_A should be regarded as concepts rather than physical quantities.

2.1.4 Antenna Radiation Efficiency

Since antennas can have certain ohmic losses, this prompts us to define radiation efficiency as the ratio of the total power radiated by the antenna to the total power accepted by the antenna at its input terminals during radiation. Hence:

$$\eta = \frac{P_{rad}}{P_{in}} = \frac{P_{rad}}{P_{rad} + P_{loss}}.$$

(2-11)

Substituting (2-8) into (2-11) yields:

$$\eta = \frac{\frac{1}{2}R_r |I_A|^2}{\frac{1}{2}R_r |I_A|^2 + \frac{1}{2}R_{loss}|I_A|^2} = \frac{R_r}{R_r + R_{loss}} = \frac{R_r}{R_A}.$$

(2-12)

(2-12) is based on the assumption that the loss mechanisms can be simply represented as a series resistance. However, (2-11) can be used in general cases.

Antenna radiation efficiency is also related to directivity and gain. The only difference between maximum gain and directivity is the power value used. Gain quantifies the fact that the input power is lost on the antenna. Using (2-4) and (2-5) and (2-11) gives:

$$G = \eta D.$$

(2-13)

2.2 Antenna Measurements

2.2.1 Antenna ranges

A facility used to measure antenna radiation characteristics is referred to as an antenna range [1], it provides a plane wave illumination of the antenna under test. Figure 2.2 shows various antenna ranges.

Source tower   **The elevated antenna range**   Test Tower   **Slant Ranges**

The compact range   Positioning Carriage   **The near-field range**
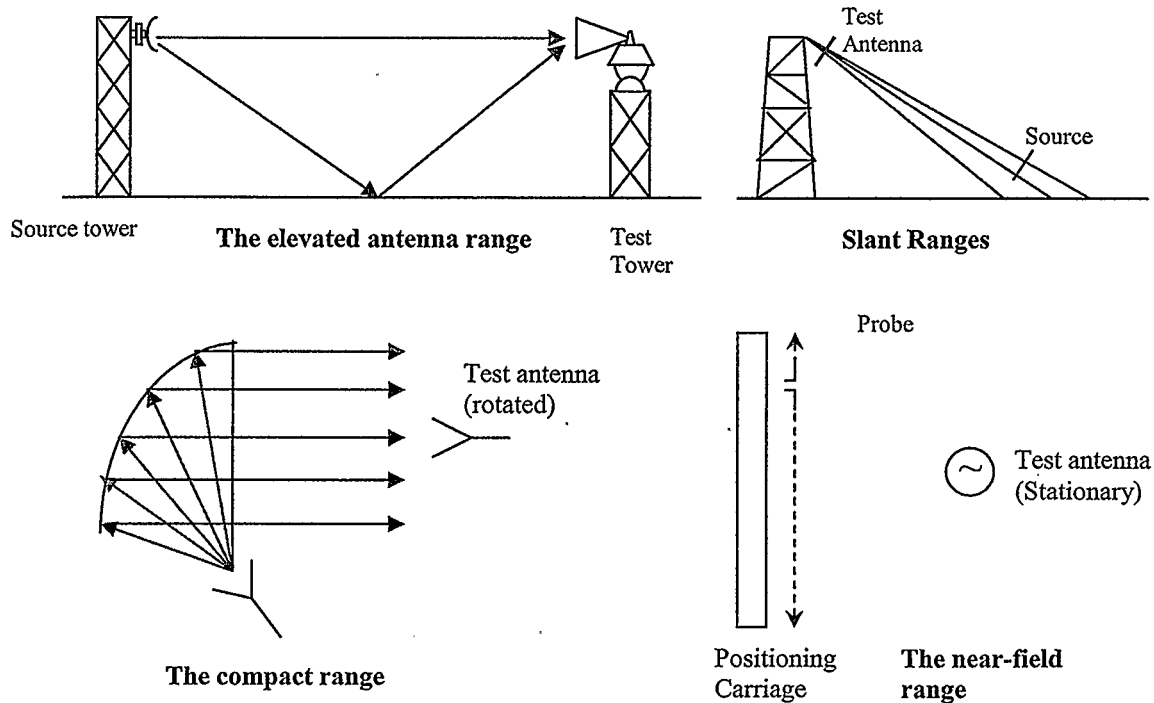
Figure 2.2 Various antennas ranges

After many years of development, near-field antenna testing has come of age and is a reliable alternative to far-field testing. It is now often the preferred approach. Conventional far-field measurement ranges often are not adequate for testing antennas accurately. Near-field measurement methods have been developed to increase accuracy, reduce costs and become independent of weather conditions.

The reactive near-field region is the region close to the antenna and up to about one wavelength away from any radiating surface. The energy decays very rapidly with distance. In the near-field region, the average power density remains fairly constant at different distances from antenna. The near-field test system measures the energy radiating

in the near-field region and converts those measurements by a Fourier transform into far-field result.

The region separation of the radiation of the antenna can be found in [2]. In practical terms, the boundary between the near-field and far-field can be expressed as [2]:

$$R = \frac{2D^2}{\lambda},$$

(2-14)

where: R = the distance measured from the antenna to the boundary,

D = the maximum dimension of the antenna,

λ = the wavelength.

Reactive near-field
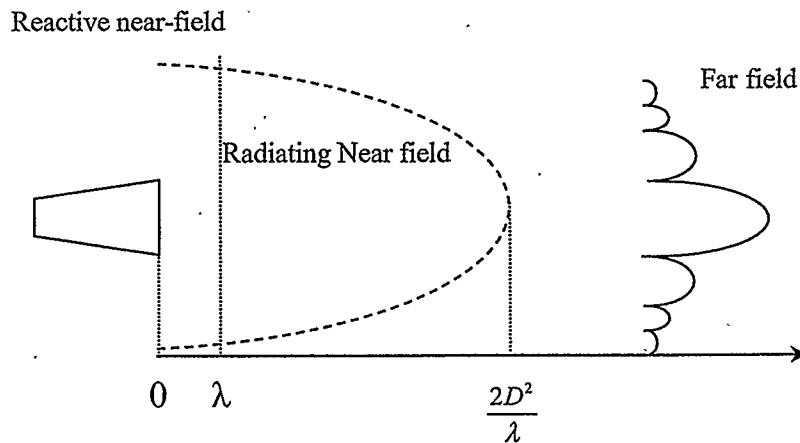
Figure 2.3 Near field and far field of antenna radiation

2.2.2 Antenna radiation pattern measurement

In general, the pattern of an antenna is a 3-D pattern. Because it is generally onerous to measure and display a three-dimensional pattern, a number of two-dimensional patterns are measured. A 2-D pattern is also referred to as pattern cut, it is obtained by

fixing one of the angles (θ or ϕ) while varying the other. The patterns of an antenna can be measured in transmitting or receiving mode. However, if the radiator is reciprocal, as is the case for most practical antennas, then either the transmitting or receiving mode can be utilized. The antenna range instrumentation usually can be classified into five categories: source antenna and transmitting system, receiving system, positioning system, recording system and data-process system.

2.2.3 Antenna gain measurement

There are two basic methods used to measure gain: absolute gain and gain comparison (gain transfer) [2]. Absolute-gain is used to calibrate antennas that can be used as standards for gain measurements. It is based on the Friis transmission formula:

$$(G_{0t})_{dB} + (G_{0r})_{dB} = 20\log_{10}\left(\frac{4\pi R}{\lambda}\right) + 10\log_{10}\left(\frac{P_r}{P_t}\right), \qquad (2\text{-}15)$$

where:

$(G_{0t})_{dB}$ = gain of the transmitting antenna (dB),

$(G_{0r})_{dB}$ = gain of the receiving antenna (dB),

P_r = received power,

P_t = transmitted power,

R = antenna separation (m),

λ = operating wavelength (m).

If the transmitting and receiving antennas are identical, then we have

$$(G_{0t})_{dB} = (G_{0r})_{dB} = \frac{1}{2}\left[20\log_{10}\left(\frac{4\pi R}{\lambda}\right) + 10\log_{10}\left(\frac{P_r}{P_t}\right)\right]. \qquad (2\text{-}16)$$

By measuring R, λ and the ratio of $\dfrac{Pr}{Pt}$, the gain can be found.

Most gain measurements are made using an antenna of known gain, called standard gain antenna. The technique is called gain comparison. Figure 2.4 shows the test arrangement. Then:

$$G_T(dB) = P_T(dBm) - P_s(dBm) + G_s(dB),$$ (2-17)

where $G_T(dB)$ and $G_s(dB)$ are the gains (in dB) of the antenna under test (AUT) and the standard gain antenna.
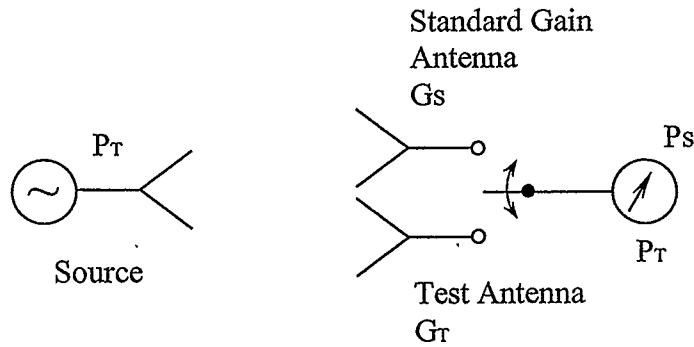
Figure 2.4 Gain comparison for gain measurement

2.2.4 Antenna directivity measurement

A simple method of determining directivity is to measure the two principal E and H plane patterns and then determine the HPBW of E and H plane. The directivity may be calculated [2] approximately as:

$$D_0 \approx \frac{32,400}{\Theta_{1d}\Theta_{2d}},$$ (2-18)

where:

Θ_{1d} = half-power beamwidth in one plane (degree),

Θ_{2d} = half-power beamwidth in a plane at a right angle to the other (degree),

E-plane is defined as "the plane contains the electrical-field vector and the direction of maximum radiation",

H-plane is defined as "the plane contains the magnetic-field vector and the direction of maximum radiation".

This equation is regarded as quite inaccurate for low gain antennas.

Chapter 3

Various Methods of Measuring of the Antenna Efficiency

The accurate measurement of antenna efficiency is a difficult task and some methods may have a substantial amount of errors. Before discussing our improved methods of antenna efficiencies measurement, it is appropriate to briefly describe other various techniques of measuring antenna efficiency.

3.1 The Gain/directivity method

The equation (2-13) prompts the gain/directivity method of efficiency measurement. In principle, this is a reliable technique, based on the definition of antenna efficiency. The gain and directivity of the AUT can be measured by a method mentioned in section 2.2.3 and 2.2.4 respectively. Since the gain and directivity are determined by independent means, the technique does not benefit from the cancellation of errors common to the measurement of both quantities [3]. In [3], Pozar measured 4 different printed antennas, all of them suffered from a variety of drawbacks of this method which may make the resulting efficiency measurement inaccurate and unreliable. The uncertainties of measurement results varied from 15%-28%.

3.2 The Radiometric method

The radiometric method [3] is another technique based on the fact that a lossy antenna pointed at a cold target will generate more noise power than a less lossy antenna pointed at the same target, because the loss mechanism of the antenna looks like a noise source at the ambient temperature. Figure 3.1 shows the experimental set-up for radiometric measurement.
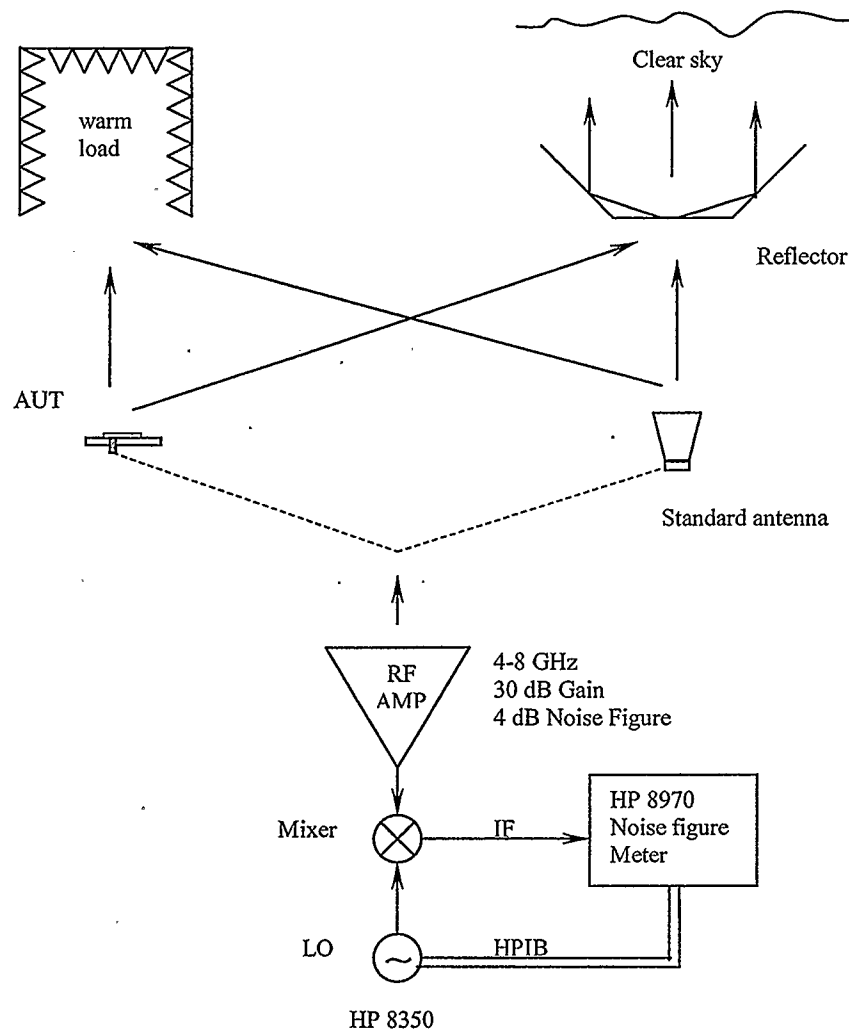
Figure 3.1 Test set-up for measuring antenna efficiency by the radiometric method [3]

The AUT is first directed toward the interior of an anechoic chamber and the noise power P_{warm} is recorded at temperature 290 K. The AUT is then directed towards the clear sky, which forms an extended cold target with a temperature of about 5 K, and the noise power P_{cold} is recorded. Then the ratio:

$$\varepsilon = \frac{P_{warm}}{P_{cold}}, \tag{3-1}$$

is a measure of the antenna efficiency and the background noise of the radiometer. A value ε much greater than unity indicates a low-noise system and an efficient antenna. To cancel the effect of system noise, the above procedure is repeated with a high efficiency antenna, such as a waveguide horn, which can be assumed to be available. If we define $\delta = \frac{P_{warm}}{P_{cold}}$ as the ratio of noise powers when this standard antenna is pointed to the anechoic chamber and the sky, then the efficiency of the test antenna can be determined as:

$$\eta = \frac{\delta(\varepsilon - 1)}{\varepsilon(\delta - 1)}. \tag{3-2}$$

In [3], Pozar realized that a number of problems can arise with this method, most of which have the effect of lowering the apparent efficiency of the AUT. In addition, the RF amplifier and mixer are required to have good noise figure. A 1-1.5 percent uncertainty in P_{warm} or P_{cold} could translate to about a 10 percent uncertainty in the measurement result of the antenna efficiency.

3.3 Resistance comparison method

This method requires the construction of a reference antenna identical to the AUT but of materials of higher or lower loss [4]. Recall (2-12), we have:

$$\eta_1 = \frac{R_{r1}}{R_{r1} + R_{loss1}}, \tag{3-3}$$

$$\eta_2 = \frac{R_{r2}}{R_{r2} + R_{loss2}}, \tag{3-4}$$

where:

η_1, η_2 = radiation efficiency of AUT and the reference antenna respectively,

R_{r1}, R_{r2} = radiation resistant of AUT and the reference antenna respectively,

R_{loss1}, R_{loss2} = resistant loss of AUT and the reference antenna respectively.

The material conductivity may affect radiation impedance slightly, i.e. $R_{r1} \doteq R_{r2}$.

Assume frequency and conductivity are both high, using surface resistance R_s to replace R_{loss}.

Define: $$\Delta = \frac{R_{loss2}}{R_{loss1}} \approx \frac{R_{s2}}{R_{s1}} = \sqrt{\frac{\mu_2 \sigma_2}{\mu_1 \sigma_1}}. \tag{3-5}$$

Incorporate (3-3), (3-4) and (3-5), yields:

$$\eta_1 = \frac{R_{in2} - \Delta \cdot R_{in1}}{R_{in1}(1 - \Delta)}, \tag{3-6}$$

$$\eta_2 = 1 - \frac{\Delta \left(R_{in1} - R_{in2} \right)}{R_{in2}(1 - \Delta)}. \tag{3-7}$$

where $R_{in1, in2}$ are the input resistors of two antennas that can be measured.

Then the efficiency can be determined using (3-6) and (3-7). The disadvantage of this method is that two identical antennas must be made of different materials. Further, the above assumptions restrict the application of this method, and it has not found much application by researchers.

3.4 The Wheeler Cap method

Wheeler set forth a method [5], where a conductive shell is placed over the antenna at the radius of transition between the antenna's near-field and its far-field. This transition radius occurs at a distance of $\dfrac{\lambda}{2\pi}$. Wheeler put a conductive sphere that reflects all of the antenna's radiation energy back into the antenna while causing minimal disturbance to the near-field. See Figure 3.2 for test apparatus.
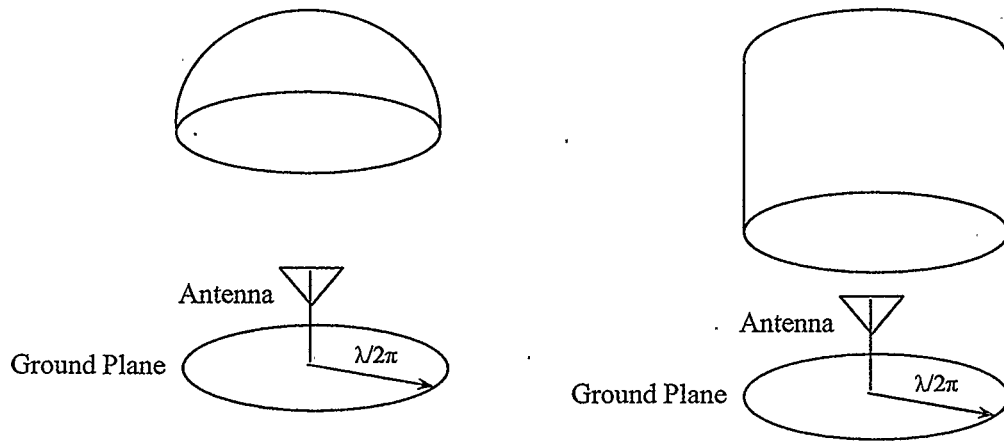
Figure 3.2 The Wheeler Cap test arrangement

If all power radiated by the antenna is reflected back by the cap and is not allowed to escape, then in the model of Figure 3.2, $R_{rad} = 0$. Assume R_{loss} remains constant with cap in place or removed.

Cap on- The radiation resistance is zero, and the reflection coefficient:

$$S_{11wc} = \frac{R_{loss} - Z_o}{R_{loss} + Z_o},\tag{3-8}$$

where

S_{11wc} = the S_{11} of AUT measured with the Wheeler Cap on,

R_{loss} = resistant loss of AUT,

Z_0 = the source resistant.

Cap off-The radiation resistance is that of the antenna radiating into free space, and the antenna reflection coefficient:

$$S_{11fs} = \frac{(R_{rad} + R_{loss}) - Z_0}{(R_{rad} + R_{loss}) + Z_0},\tag{3-9}$$

where:

R_{rad} = radiation resistant of AUT,

S_{11fs} = the S_{11} of AUT measured in free space.

From (3-8) and (3-9), we get:

$$\frac{R_{loss}}{Z_0} = \frac{1 + S_{11wc}}{1 - S_{11wc}},\tag{3-10}$$

and

$$\frac{(R_{rad} + R_{loss})}{Z_0} = \frac{1 + S_{11fs}}{1 - S_{11fs}}.\tag{3-11}$$

And the efficiency is:

$$\eta = \frac{R_{rad}}{R_{rad}+R_{loss}} = \frac{\left(\dfrac{1+S_{11fs}}{1-S_{11fs}}\right)-\left(\dfrac{1+S_{11wc}}{1-S_{11wc}}\right)}{\left(\dfrac{1+S_{11fs}}{1-S_{11fs}}\right)} = 1-\frac{\left(1-S_{11fs}\right)\left(1+S_{11wc}\right)}{\left(1+S_{11fs}\right)\left(1-S_{11wc}\right)}. \qquad (3\text{-}12)$$

The above derivation assumes that radiation and loss resistances are not accompanied by any reactive impedances (i.e. reactance). Therefore, the S_{11wc} and S_{11fs} measurements need to be made at the antenna's resonance frequency which may not be same as the antenna's actual operating frequency. Note that the antenna's efficiency will vary with frequency. However, Wheeler does not provide for a method to ensure that the above assumption is met. The Wheeler cap provides a convenient and reasonably accurate method of determining antenna efficiency and is widely used. But the Wheeler method involves the assumption that the loss in the antenna may be modeled as a resistance in series with the radiation resistance. Therefore, an alternative method should be found to measure efficiency to remove this limitation.

Chapter 4

Improved methods of Antenna Efficiency Measurement

Since the previously mentioned methods as well as other available methods developed by other researchers have potential for a substantial amount of error or depend on certain assumptions, researchers, at this institution, have developed improved methods [6] which potentially have high accuracy. The method will now be discussed. The research will be extended beyond that described in reference [6] by purposely operating the waveguide and a new structure in a multimode condition.

4.1 Basic Theory

As shown in 3.4, equations (3-8) and (3-9) (which are used by the Wheeler cap method), can not be correctly used if radiation and loss resistances are accompanied by reactance, or if the equivalent circuit of the antenna is not a pure series circuit, as is the case for most practical antennas.

In this work, the antenna is considered to be a linear two-port network appearing between an input transmission medium and an output transmission medium. The input transmission medium is often a coaxial line, and the output medium is free space. The two-port network represents the complete behavior of the antenna with respect to stored electric-field energy, stored magnetic-field energy, and heat loss. Figure 4.1 shows the two-port nodes representing the antenna. The load resistance, Z_L, is the impedance seen

by the antenna at its output when immersed in free space. A matched termination for the
antenna may be considered to be free space at an infinite distance.
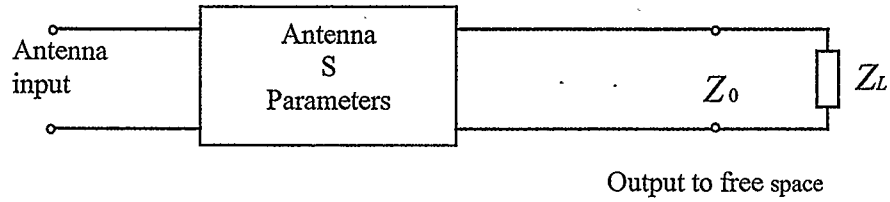
Figure 4.1 The antenna model in free space

The scattering matrix provides a complete description of the two-port (or multiport)
network. Consider a two-port network shown in Figure 4.2.
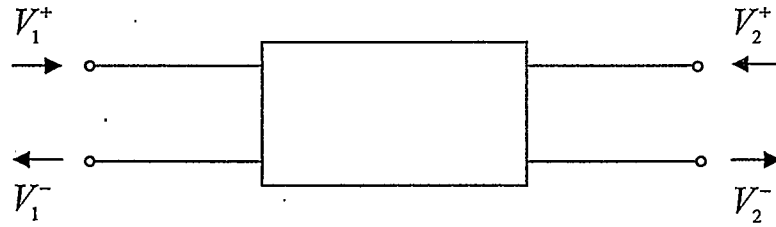
Figure 4.2 The two port network

where V_1^+ and V_2^+ are the amplitude of the voltage waves incident on port 1 and port 2
respectively, and V_1^- and V_2^- are the amplitude of the voltage waves reflected from port
1 and port 2 respectively. The scattering parameters, or $[S]$ matrix, is defined in relation
to these incident and reflected voltage waves as:

$$\begin{bmatrix} V_1^- \\ V_2^- \end{bmatrix} = \begin{bmatrix} S_{11} & S_{12} \\ S_{21} & S_{22} \end{bmatrix} \begin{bmatrix} V_1^+ \\ V_2^+ \end{bmatrix} . \qquad (4\text{-}1)$$

All elements can be determined as:

$$S_{11} = \left. \frac{V_1^-}{V_1^+} \right|_{V_2^+ = 0} , \qquad (4\text{-}2)$$

$$S_{21} = \left. \frac{V_2^-}{V_1^+} \right|_{V_2^+ = 0} , \qquad (4\text{-}3)$$

$$S_{12} = \left. \frac{V_1^-}{V_2^+} \right|_{V_1^+ = 0} , \qquad (4\text{-}4)$$

$$S_{22} = \left. \frac{V_2^-}{V_2^+} \right|_{V_1^+ = 0} . \qquad (4\text{-}5)$$

Thus, S_{11} is the reflection coefficient seen looking into port 1 when port 2 is terminated in matched load. S_{21} is the transmission coefficient from port 2 to port 1 when port 2 is terminated in matched load.

Now, applying the signal source to the antenna modeled in Figure 4.1 yields the following Figure 4.3.
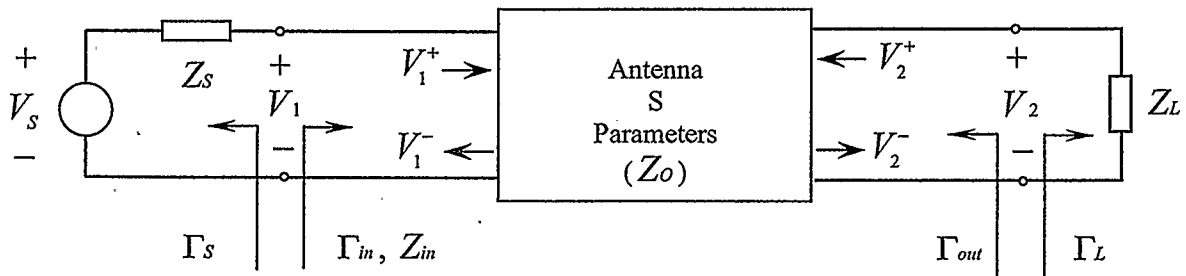
Figure 4.3 The antenna model in free space with an applied source voltage

Where: V_s = source open circuit voltage,

Z_s = source impedance,

Z_{in} = impedance seen looking toward the input port,

Z_o = characteristic impedance reference for the S parameter of the network,

Γ_{in} = the reflection coefficient at the antenna's input terminal,

Γ_L = the reflection coefficient by free space at the antenna's output terminal,

Γ_s = the reflection coefficient seen looking toward the source.

The antenna efficiency can be defined as the power delivered to the load relative to the power delivered to the network. In active microwave theory, this is often called Power Gain [7]. This gain is independent of the source impedance Z_s.

From transmission line theory, the reflection coefficient seen looking into the source is:

$$\Gamma_s = \frac{Z_s - Z_0}{Z_s + Z_0}, \tag{4-6}$$

while the reflection coefficient seen looking into the input of the networks is:

$$\Gamma_{in} = \frac{Z_{in} - Z_0}{Z_{in} + Z_0}. \tag{4-7}$$

Solving for Z_s and Z_{in} from (4-6) and (4-7) gives:

$$Z_s = Z_0 \frac{1 + \Gamma_s}{1 - \Gamma_s}, \tag{4-8}$$

$$Z_{in} = Z_0 \frac{1 + \Gamma_{in}}{1 - \Gamma_{in}}. \tag{4-9}$$

Dividing (4-8) by (4-9) yields:

$$\frac{Z_s}{Z_{in}} = \frac{(1+\Gamma_s)(1-\Gamma_{in})}{(1-\Gamma_s)(1+\Gamma_{in})}.$$ (4-10)

By voltage division,

$$V_1 = V_s \frac{Z_{in}}{Z_{in}+Z_s} = V_1^+ + V_1^- = V_1^+(1+\Gamma_{in}),$$ (4-11)

from (4-11) and solving for the amplitude of the voltage wave incident on the input

terminal of the antenna is:

$$V_1^+ = \frac{Z_{in}V_s}{(Z_{in}+Z_s)(1+\Gamma_{in})} = \frac{V_s}{\left(1+\dfrac{Z_s}{Z_{in}}\right)(1+\Gamma_{in})}.$$ (4-12)

Substituting (4-10) to (4-12) yields:

$$V_1^+ = \frac{V_s(1-\Gamma_s)}{2(1-\Gamma_s\Gamma_{in})}.$$ (4-13)

If peak values are assumed for all voltages, the average voltage power delivered to the

network is:

$$P_{in} = \frac{1}{2Z_0}\left|V_1^+\right|^2\left(1-\left|\Gamma_{in}\right|^2\right) = \frac{\left|V_s\right|^2}{8Z_0}\frac{\left|1-\Gamma_s\right|^2}{\left|1-\Gamma_s\Gamma_{in}\right|^2}\left(1-\left|\Gamma_{in}\right|^2\right).$$ (4-14)

From (4-1), we have:

$$V_2^- = S_{21}V_1^+ + S_{22}V_2^+,$$ (4-15)

where: $$\Gamma_L = \frac{V_2^-}{V_2^+}.$$ (4-16)

Combining (4-15) and (4-16) and solving for V_2^- which is the amplitude of the voltage incident on the load gives:

$$V_2^- = \frac{S_{21}V_1^+}{1 - S_{22}\Gamma_L}.$$ (4-17)

Substituting (4-13) into (4-17) yields:

$$V_2^- = \frac{V_S(1 - \Gamma_s)S_{21}}{2(1 - \Gamma_s\Gamma_{in})(1 - S_{22}\Gamma_L)}.$$ (4-18)

The average power delivered to the load is:

$$P_L = \frac{1}{2Z_0}\left|V_2^-\right|^2\left(1 - \left|\Gamma_L\right|^2\right).$$ (4-19)

Substituting (4-18) into (4-19), we get:

$$P_L = \frac{V_S^2\left|1 - \Gamma_s\right|^2 S_{21}\left(1 - \left|\Gamma_L\right|\right)^2}{8Z_0\left|1 - \Gamma_s\Gamma_{in}\right|^2\left|1 - S_{22}\Gamma_L\right|^2}.$$ (4-20)

The power gain, i.e., the radiation efficiency, can be then expressed as

$$\eta = G = \frac{P_L}{P_{in}} = \frac{\left|S_{21}\right|^2\left(1 - \left|\Gamma_L\right|^2\right)}{\left(1 - \left|\Gamma_{in}\right|^2\right)\left|1 - S_{22}\Gamma_L\right|^2},$$ (4-21)

where G = power gain,

P_L = The power delivered in the load, i.e., the power radiated by the antenna,

P_{in} = The power delivered to the input of the two-port network, i.e., the power fed into the antenna.

The relation between Γ_L and Γ_{in} can be found from Figure 4.4
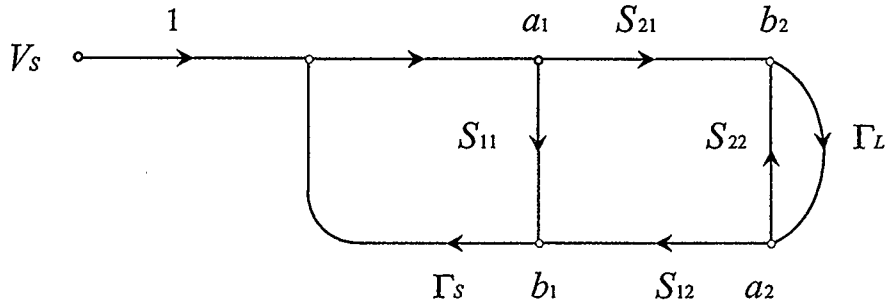
Figure 4.4 Signal flow graph for the two-port network with a general source

Applying Mason law, the Γ_{in} can be directly written as:

$$\Gamma_{in} = \frac{b_1}{a_1} = \frac{S_{11}(1 - S_{22}\Gamma_L) + S_{21}S_{12}\Gamma_L}{1 - S_{22}\Gamma_L} = S_{11} + \frac{S_{21}S_{12}\Gamma_L}{1 - S_{22}\Gamma_L}. \qquad (4\text{-}22)$$

Substituting (4-22) into (4-21) gives the efficiency as:

$$\eta = \frac{|S_{21}|^2 \left(1 - |\Gamma_L|^2\right)}{\left|1 - S_{22}\Gamma_L\right|^2 - \left|(S_{12}S_{21} - S_{11}S_{22})\Gamma_L + S_{11}\right|^2}. \qquad (4\text{-}23)$$

As free space is considered to be a matched termination for the antenna, $\Gamma_L = 0$, and

(4-23) simplifies to:

$$\eta = \frac{|S_{21}|^2}{1 - |S_{11}|^2}. \qquad (4\text{-}24)$$

It can be shown that equation (4-24) is free of the restrictions which apply to the

Wheeler Cap method. It prompts a method of determining the antenna efficiency by

measuring the magnitude of the S_{11} and S_{21}. We call this method a transmission method

since the transmission parameter S_{21} will be measured.

4.2 Transmission Measurement Method

The measurement technique is based on the concept that a small antenna can be placed in a waveguide without disturbing the near fields or the current and voltage distributions (or the stored electric field and magnetic field distribution) within the antenna. In this way, the two-port network of the antenna is the same in free space as in the waveguide. Since the dimensions of the waveguide are about $3/8\,\lambda$ by $3/4\,\lambda$, a good clearance from its walls can be achieved for an electrically small antenna. The antenna is mounted on the bottom wall of the waveguide that acts as a ground plane, which makes the efficiency-measurement method very suitable for measuring ground-plane mounted antennas. The Figure 4.5 shows the test arrangement.

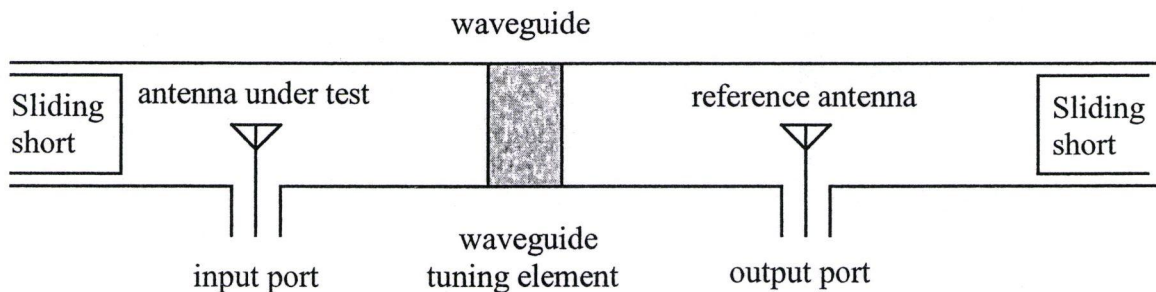Figure 4.5 The waveguide arrangement for the transmission efficiency measurement

The waveguide environment should provide a load impedance to the antenna that is a good approximation of the load impedance offered by free space. Generally, when tuned, the waveguide environment provides a wide range of impedances to a structure placed within it. Sliding shorts are placed at each end of the waveguide, so that there is no signal

leakage. The position of the sliding shorts is adjusted in order to achieve proper impedance matching of the antenna under test. The tuning element shown in Figure 4.5 may be used to achieve further matching. The two sliding shorts, and any waveguide tuning element are adjusted such that the measured S_{11wg} of the antenna in the waveguide is the same as the S_{11fs} of the antenna measured in free space, at the frequencies of interest. The equivalence between S_{11wg} and S_{11fs} will only occur over a limited frequency span. This will affect the measurement accuracy if the measurements are made over a wide frequency range.

4.3 Reflection Measurement Method

In this method, the magnitude of the forward-scattering parameter S_{21} is calculated rather than measured directly. The test setup is shown in Figure 4.6.
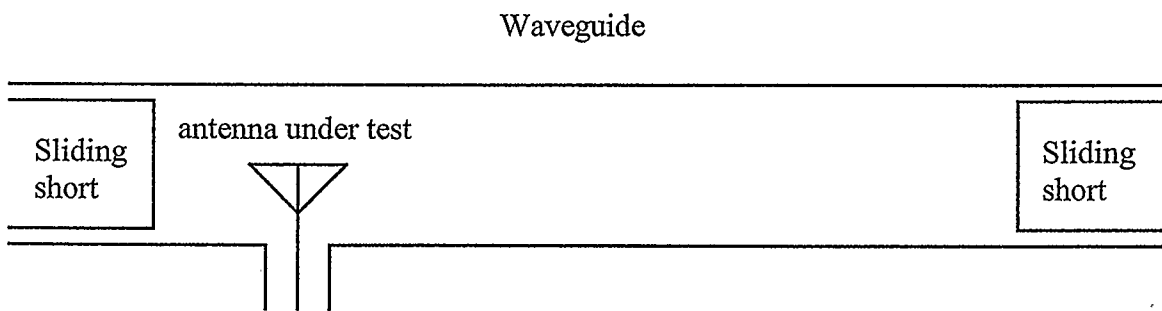
Waveguide

Figure 4.6 The waveguide arrangement for the reflection efficiency measurement

The test setup uses the same waveguide, but with the reference antenna removed, so that only the input reflection scattering parameter S_{11wg} can be observed. If S_{11wg} is measured for a number of different positions of the output sliding short (the one at the right hand) as it is moved along the length of the waveguide, then the measured S_{11wg} will describe a circle, when plotted on the Smith chart or polar plot. The center and radius of the circle are dependent on the two-port S parameters of the antenna. For the Nth measurement, the relation between the measured reflection coefficient, $S_{11wg,N}$, and the antenna's two-port S parameters may be written as:

$$S_{11wg,N} - S_{11,fs} = \frac{S_{21}S_{12}\exp(j\theta_N)}{1 - S_{22}\exp(j\theta_N)}, \tag{4-25}$$

where θ_N is the phase angle of the $S_{11wg,N}$.

Now, defining two new variables:

$$\Delta S_{max} = \max\left\{\left|S_{11wg} - S_{11fs}\right|\right\}, \tag{4-26}$$

$$\Delta S_{min} = \min\left\{\left|S_{11wg} - S_{11fs}\right|\right\}. \tag{4-27}$$

Substituting (4-26) and (4-27) into (4-25) yields two new expressions:

$$\Delta S_{max} = \frac{|S_{21}S_{12}|}{1 - |S_{22}|}, \tag{4-28}$$

$$\Delta S_{min} = \frac{|S_{21}S_{12}|}{1 + |S_{22}|}, \tag{4-29}$$

which can be rearranged to give:

$$1 - |S_{22}| = \frac{|S_{21}S_{12}|}{\Delta S_{max}}, \tag{4-30}$$

$$1 + |S_{22}| = \frac{|S_{21}S_{12}|}{\Delta S_{min}}.$$

(4-31)

Given that $S_{21} = S_{12}$ for a passive reciprocal antenna, as is the case for most antennas,

Equations (4-30) and (4-31) can be summed and transformed to give:

$$|S_{21}|^2 = \frac{2}{(\Delta S_{max})^{-1} + (\Delta S_{min})^{-1}}.$$

(4-32)

Substituting (4-32) into (4-24) yields (4-33), a new expression of antenna efficiency that

than can be easily related to the measurement of the antenna's reflection coefficient in the

waveguide:

$$\eta = \frac{2}{(\Delta S_{max})^{-1} + (\Delta S_{min})^{-1}} \cdot \frac{1}{1 - |S_{11fs}|^2}.$$

(4-33)

At a single frequency, a minimum of three measurements of S_{11wg} (three different

positions of the sliding short), is required to determine the circle. A large number of

measurements are desirable for the purpose of accuracy improvement. If efficiencies over

a range of frequency are required, it is convenient to determine each circle at each

frequency. A MATLAB program was written to fit a circle to the measured S_{11wg} with

minimum square error. The measured values of S_{11fs} are then combined with the circle to

extract the ΔS_{max} and ΔS_{min}. The procedure is shown as Figure 4.7.
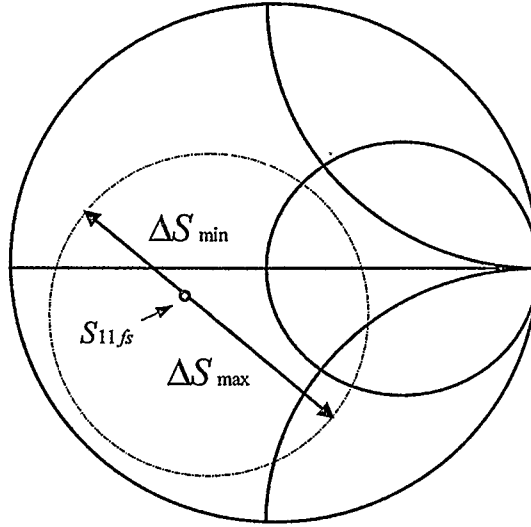
Figure 4.7 The determination of ΔS_{max} and ΔS_{min}

In the reflection method the magnitude of S_{21} is measured indirectly, therefore it does not require a fine matching of the waveguide-load impedance to the free-space impedance as in the transmission method.

The reflection method does not suffer the restriction of the Wheeler cap method either. However, it can be regarded as a generalized Wheeler cap method. Taking the original Wheeler cap method assumptions to be true, at antenna resonance, $Z_{fs} = R_r + R_{loss}$. When the cap is put on, the input impedance is measured at the same frequency, yielding $Z_{wg} = R_{loss} + jX$, where X is unknown imaginary part. To simply the mathematics, we can use a Z_0 value of $R_r + R_{loss}$ to normalize the impedance. Refer to Figure 4.8.

From the Smith chart, we see that:

$$\Delta S_{max} = 1,$$

(4-34)

$$\Delta S_{min} = \left| \frac{R_{loss} - Z_0}{R_{loss} + Z_0} \right| = \frac{R_{loss} - (R_r + R_{loss})}{R_{loss} + R_r + R_{loss}} = \frac{R_r}{2R_{loss}},$$ (4-35)

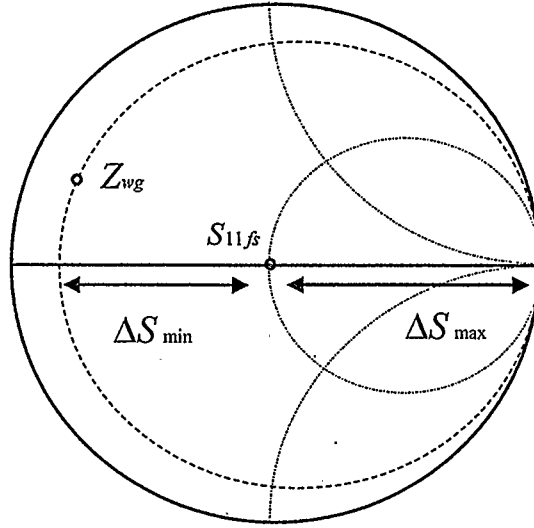$$S_{11fs} = 0.$$ (4-36)

Figure 4.8 The input impedance

Substituting (4-34), (4-35) and (4-36) into (4-33) yields:

$$\eta = \frac{2}{\left(\dfrac{R_r}{R_r + 2R_{loss}} \right)^{-1} + 1} = \frac{R_r}{R_r + R_{loss}}.$$ (4-37)

in which Equation (4-37) is used by the Wheeler cap method.

4.4 Waveguide Cavity Construction

The waveguide is built with cross-sectional internal dimensions of 302 mm×173 mm, with a length of 1220 mm, which gives a practical operation frequency roughly above 500 MHz.

The sliding shorts are best described as open-top boxes, with cross-sectional dimensions of 295×170 mm. The bottom of the box is a copper sheet, and the sides are made of copper strips with a width of approximately 15mm, alternating with air gaps of about 15mm. Spacing insulators are used to hold the sliding shorts off the waveguide walls, so that a choke-short action is achieved when installed in the waveguide. The conductor strips act as microstrip lines of a quarter wavelength (with air dielectric) with their outer ends open-circuited, which provides a short circuit at the inner face of the sliding short. Therefore, when measuring at a very large frequency range, the length of the sliding shorts and the strips must be varied in order to keep with the strips about a quarter wavelength in length. Some signal power can escape at non-resonant frequencies, causing the antenna under test to have a reduced measured efficiency at these particular signal frequencies. Reduction of the gap between the waveguide walls and the sliding shorts are expected to reduce energy leakage at all frequencies. These sliding shorts are inserted into the waveguide with a calibrated rod, to provide repeatable measurement. The Figure 4.9 shows the construction of the sliding short.
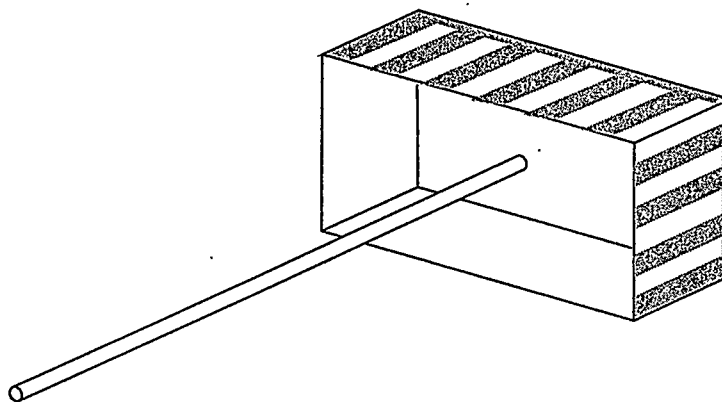

Figure 4.9 The construction of the sliding short

The reference antenna is constructed from a copper sheet, in the shape of an inverted isosceles triangle, with an attached rectangle. The apex of the triangle is attached to the center pin of a coaxial connector. This is called a vane antenna in this thesis. Three vane antennas with different dimensions were built for test as shown in Figure 4.10.
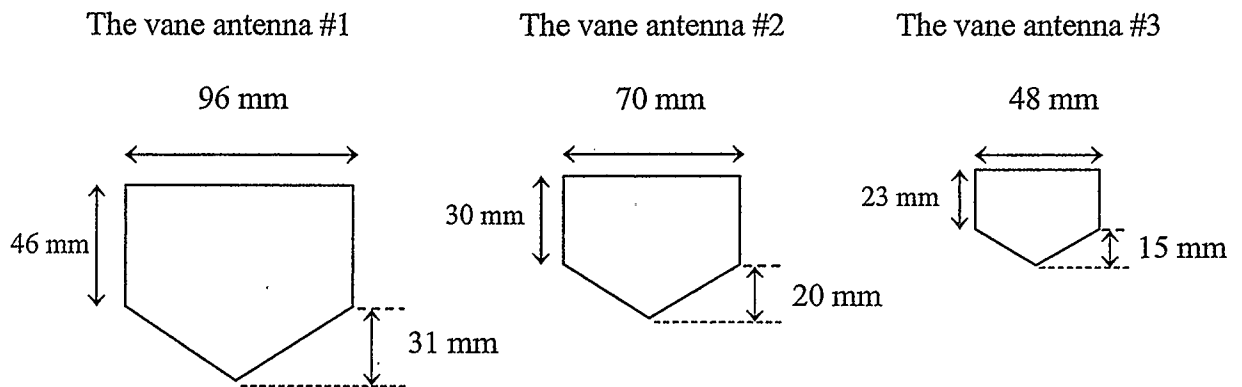
The vane antenna #1   The vane antenna #2   The vane antenna #3

96 mm   70 mm   48 mm

46 mm   30 mm   23 mm

31 mm   20 mm   15 mm

Figure 4.10 The construction of three vane antennas

4.5 Measurements and Measurement Results

The efficiency measurements were carried out using an HP8719ES automatic network analyzer, in the frequency range from 600 MHz to 1 GHz at 401 frequencies. Sixteen times averaging was used to reduce the effects of noise. Since the reflection method is likely to be more accurate than the transmission method [6], more measurements are conducted on the reflection method.

4.5.1 The measurement of the reference antenna

The vane antenna, a copper vane with a large surface area over which the current flows, should be expected to have a very high radiation efficiency. Therefore, the measurements of the vane antenna #1 were firstly conducted with the reflection method in the rectangular waveguide. The measurements of S_{11wg} was taken with the waveguide short in different positions. A minimum of three positions are needed to define the circle. A large number of positions allows a more accurate definition of the circle at each frequency. We measured ten S_{11wg} values with the waveguide short in ten positions at each frequency sample. Refer to Figure 4.11 to see the measurement result.
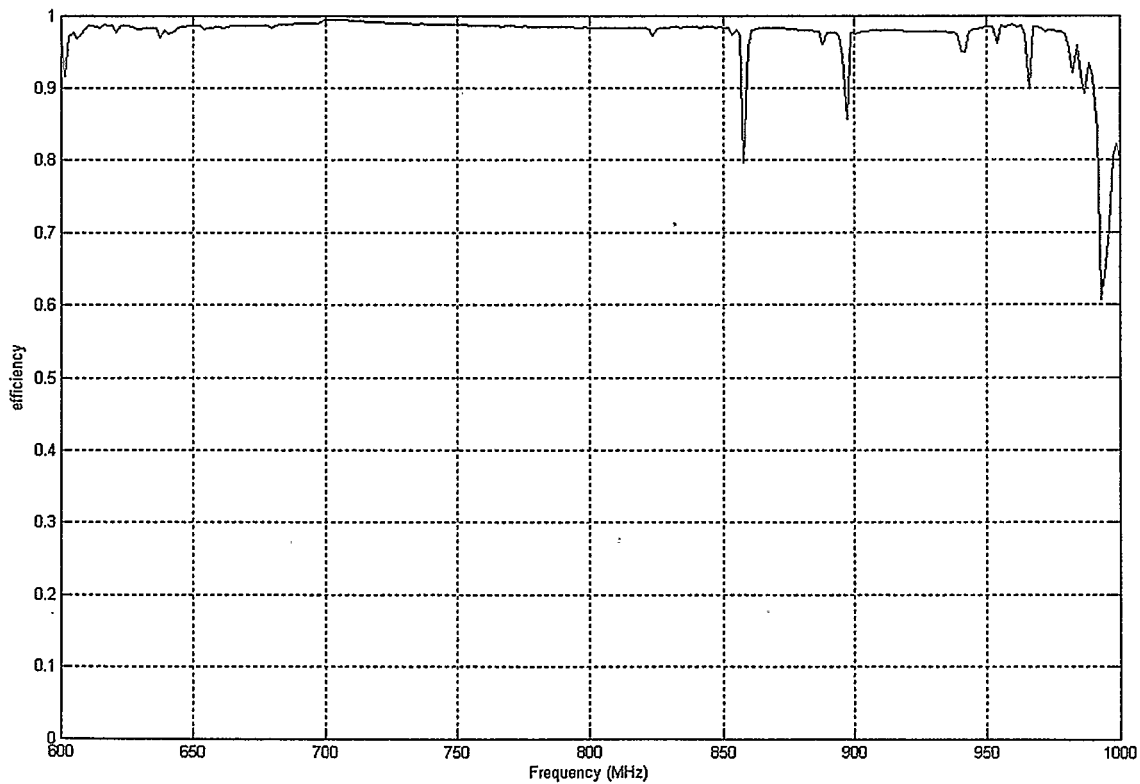

Figure 4.11 Measured efficiency of vane antenna #1 in a waveguide

4.5.2 Measurement of the different wire monopole antennas

We measured three different quarter wave monopoles. All monopoles had a length of 85 mm and were made of copper. Examination of the results shown on Figure 4.12 shows that the larger diameter wires tend to have a measurably higher efficiency.
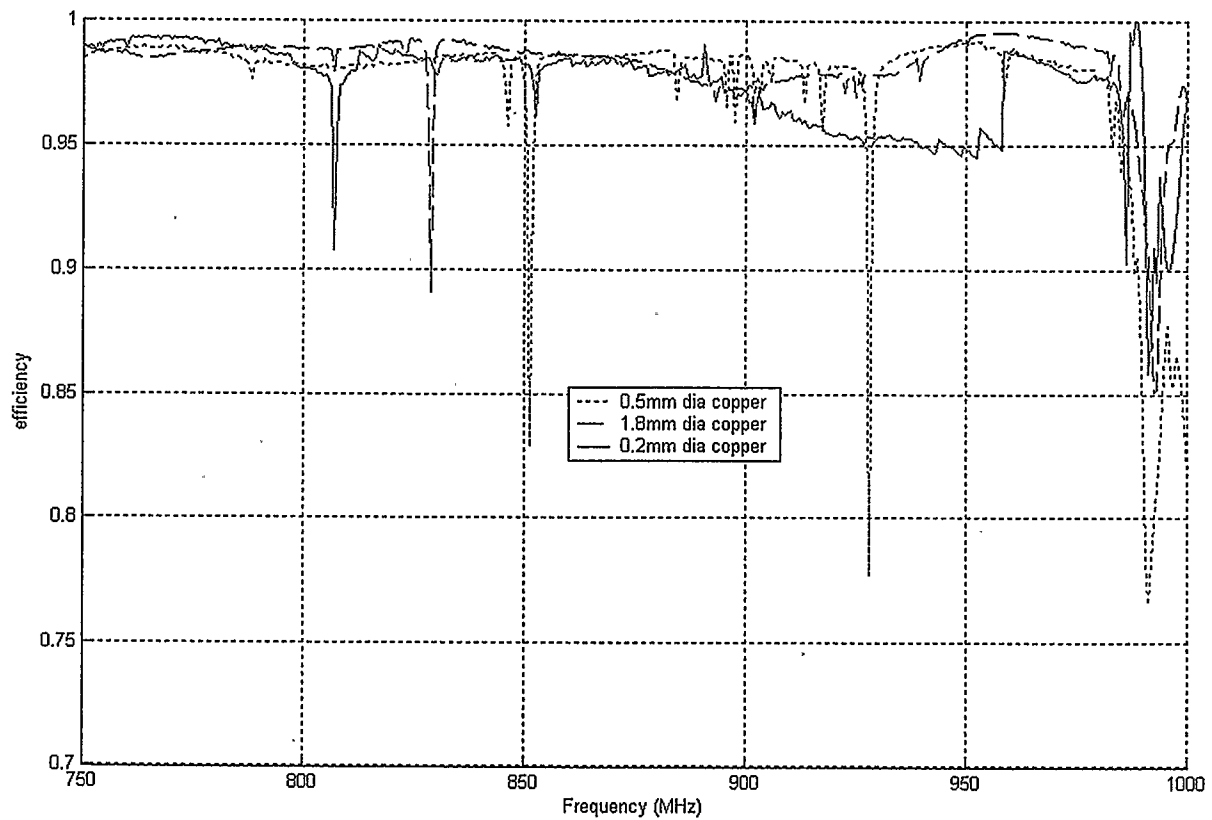

Figure 4.12 The efficiencies of different wire monopoles measured in the waveguide

4.5.3 Rectangular waveguide losses at multi-mode cut-off frequencies

There are efficiency notches shown in Figure 4.11 and Figure 4.12. In addition to possible energy leakage from the sliding shorts, they are also caused by the attenuation of various higher modes in the waveguide that can be excited by the antenna placed in the waveguide.

Energy launched into a higher order mode near its cutoff frequency will have significant losses which will show up as a reduced antenna efficiency. The attenuation α can be expressed in [8] as:

$$\alpha = \frac{2R_m}{b\eta(1-k_{cmn}^2/k_0^2)}\left[\left(1+\frac{b}{a}\right)\frac{k_{cmn}^2}{k_0^2}+\frac{b}{a}\left(\frac{\varepsilon_{0m}}{2}-\frac{k_{cmn}^2}{k_0^2}\right)\frac{m^2ab+n^2a^2}{m^2b^2+n^2a^2}\right], \quad (4\text{-}38)$$

where:

a and b are the dimension of rectangular waveguide,

$$\eta = 120\pi, \quad (4\text{-}39)$$

$$k_{cmn}^2 = \left(\frac{m\pi}{a}\right)^2+\left(\frac{n\pi}{b}\right)^2, \quad (4\text{-}40)$$

$$k_0^2 = \omega\sqrt{\mu_0\varepsilon_0}, \quad (4\text{-}41)$$

$$R_m = \sqrt{\frac{\omega\mu_0}{2\sigma}}, \quad (4\text{-}42)$$

$$\varepsilon_{0m} = 1 \text{ for } m=0 \text{ and } \varepsilon_{0m} = 2 \text{ for } m \neq 0. \quad (4\text{-}43)$$

The waveguide losses can be plotted as a function of frequency according to the dimension of our rectangular waveguide as following Figure 4.13 and Figure 4.14.
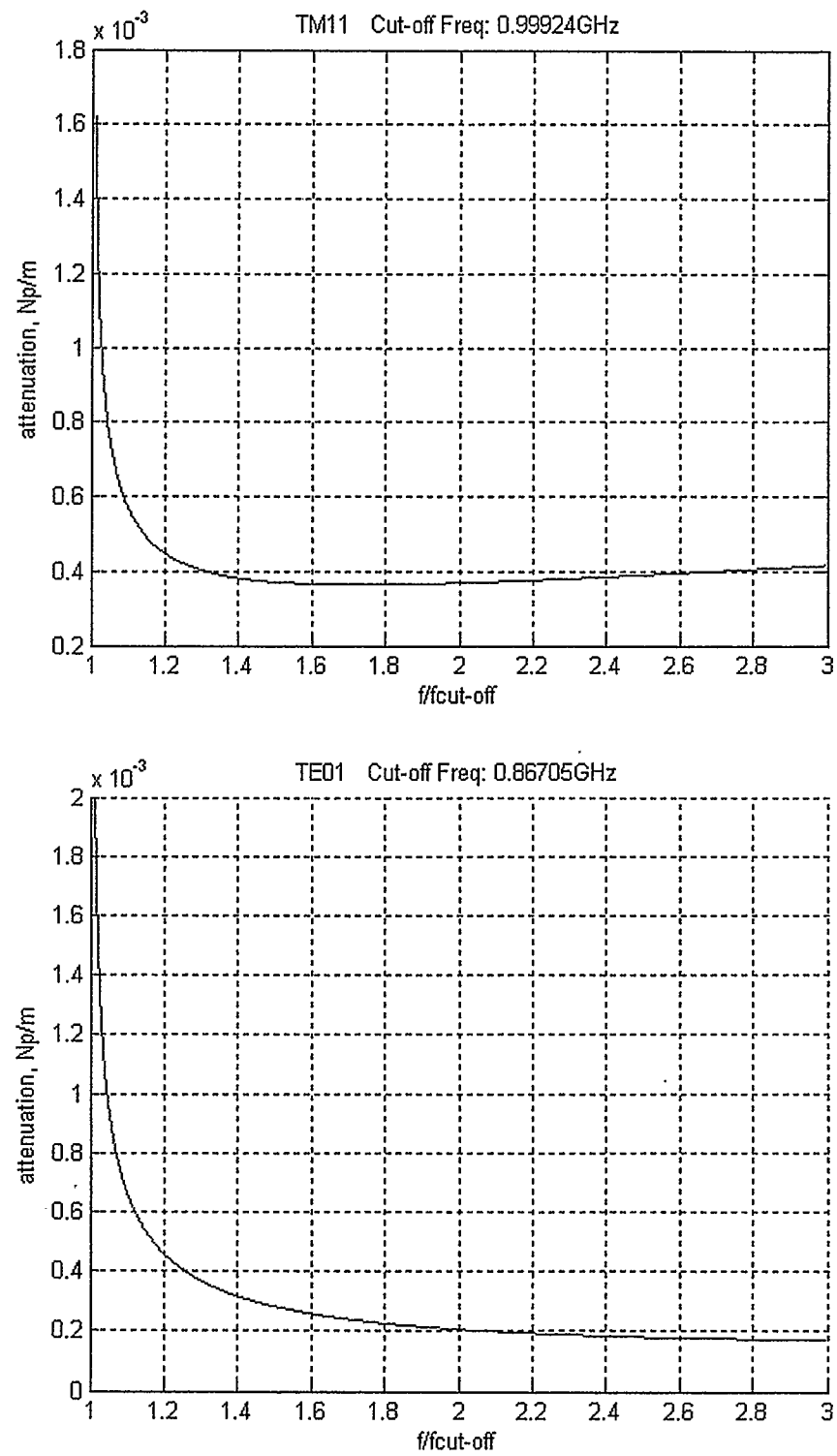
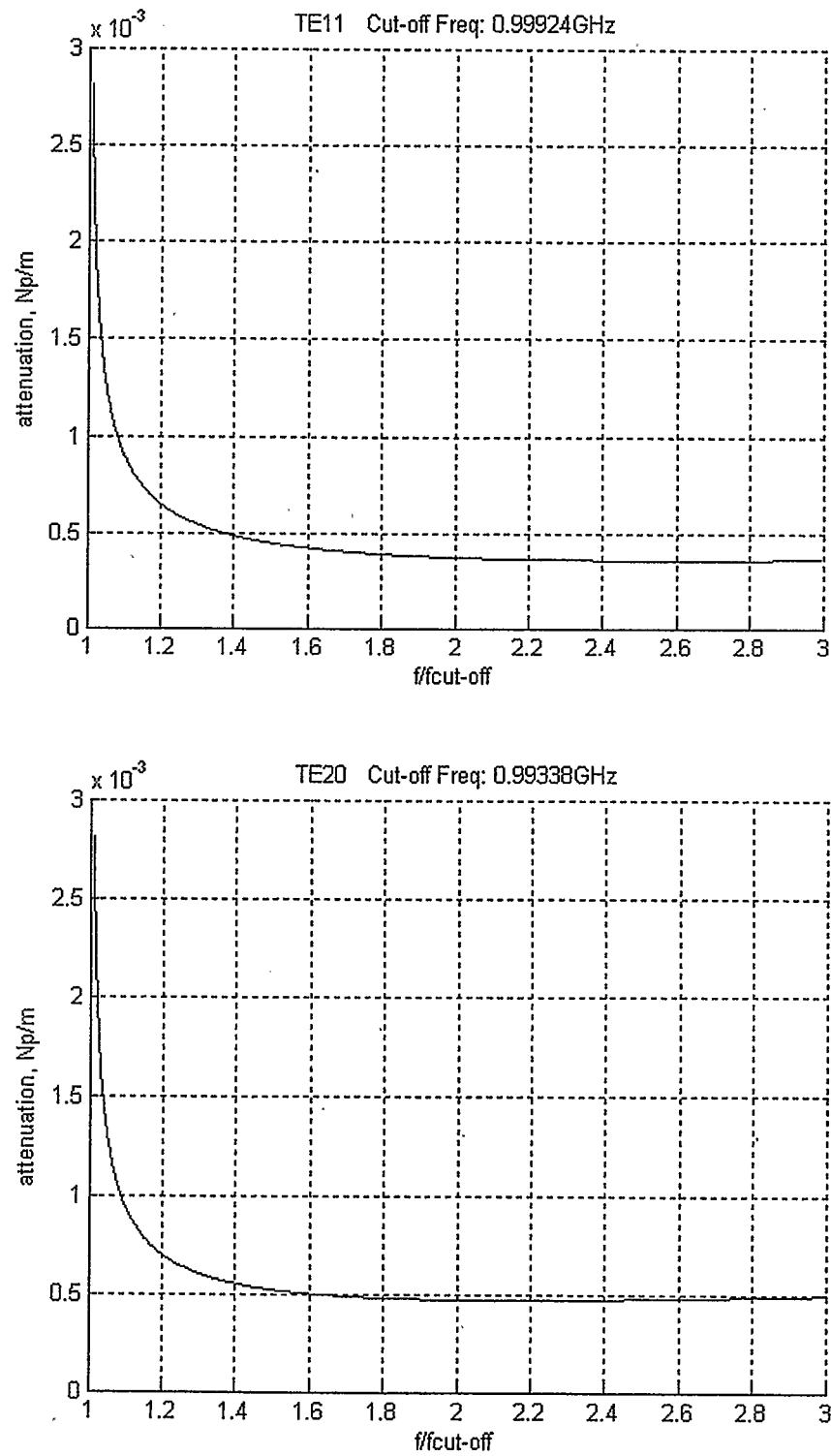Figure4.13 Waveguide attenuation for modes TM11 and TE01

Figure 4.14 Waveguide attenuation for modes TE11 and TE20

From the above figures, it can be seen that the attenuation of each mode will be very high when the operating frequency approaches the respective cut-off frequency. These multimode efficiency notches have been attributed to coupling resistances [9]. The waveguide that we built has higher order mode cutoff frequencies of 867, 993 and 999 MHz which accounts for most of the efficiency notches shown on Figure 4.11 and Figure 4.12. In addition to the multimode losses, the energy leakages from the both sliding shorts contribute to reduced efficiency.

It should be noted that the waveguide was constructed in a non ideal way. The internal slot at the junction of the top plate and bottom bent plate, as shown in Figure 4.15, can be expected to lower the cutoff frequencies of the various modes.
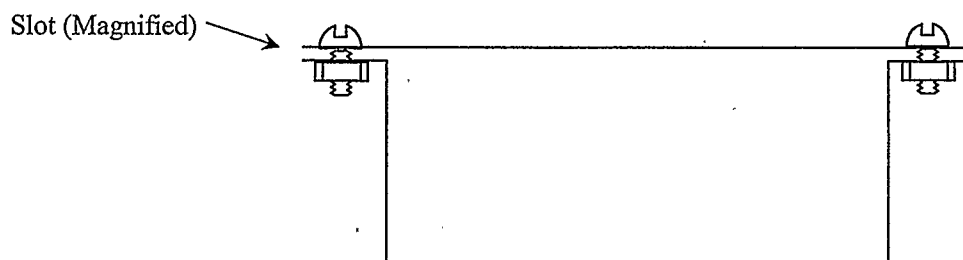

Figure 4.15 The cross section of the waveguide

In addition, the waveguide we built is physically vulnerable. When the sliding short was moved from one position to another, it would sometimes rotate slightly about a vertical axis causing less or more conversion of the dominant mode energy into higher order modes energies which reduced measurement accuracy.

Chapter 5

Efficiency Measurement Using a Precision Waveguide

The waveguide built in Chapter 4 suffers from its structural flexibility and varying cross-sectional dimensions along its length. In addition, the larger dimension of the cross section results in the lower cutoff frequency of the dominant mode. Since the waveguide efficiency measurement has multi-mode losses described in section 4.5.3, the upper limit of the measurement frequency is restricted. A precision rectangular waveguide was then constructed with smaller dimensions and substantial physical rigidity. The interior of the waveguide was plated with a high conductivity and oxidation resistant metal.

5.1 The construction of the precision waveguide

The precision rectangular waveguide is made of brass and the inner planes are plated with gold for the purpose of reducing loss. The thickness of the side walls of the waveguide is 6 mm to ensure a strong structure. The waveguide is constructed with internal dimensions of 200 mm × 100 mm, with a length of 910 mm. The cut-off frequency of dominant mode TE_{10} is 750 MHz and the next three over-mode cut-off frequencies are, 1.5 GHz, 1.67 GHz and 2.12 GHz. Therefore, the AUT can be measured in the frequency range of 760 MHz to 1.5 GHz without the generation of higher modes. Figure 5.1 shows the construction of the precision waveguide with the sliding short

inserted. The sliding short is also made of brass plate and is also gold plated. It has a five

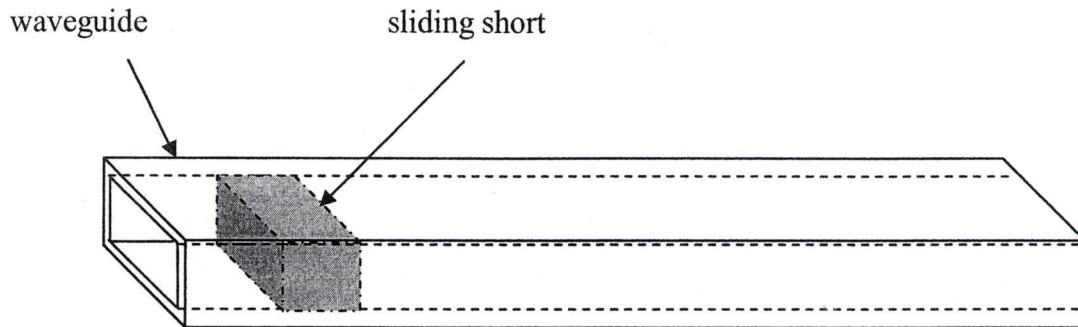sided rectangular box shape. The open end faces the open end of the waveguide.

Figure 5.1 The precision waveguide with the sliding short inserted

5.2 Fundamental mode measurement results

Within frequency range of 750 MHz to 1.5 GHz, only the fundamental mode

TE_{10} is propagated in the waveguide. In practice, the measurements should be taken

between 760 MHz to 1.3 GHz to ensure that only the fundamental mode exists for the

purpose of avoiding multi-mode losses discussed in section 4.5.3.

5.2.1 The vane antenna

The precision waveguide has smaller dimensions than the waveguide used in Chart

4. To ensure a sufficient clearance between the AUT and the inner walls of the precision

waveguide, the vane antennas #2 in Figure 4.10, which is smaller than the vane antenna

#1, is used for fundamental mode efficiency measurements. Wheeler suggests that the

radius of 0.159λ for a spherical shell for an antenna of zero dimensions is sufficient to have less interference with the antenna's near field. For operation at 1 GHz, the precision waveguide provides a clearance of 0.16λ for the vane antenna #2, which provides sufficient clearance.

The measurement result of the vane antenna #2 is shown in Figure 5.2. There are no efficiency notches in the result because no higher order modes are propagated within the measurement frequency from 760 MHz to 1300 MHz. The vane antenna measured in the precision waveguide has smaller dimensions than the vane antenna mentioned in Chapter 4. This will result in the lower efficiency for the smaller vane antenna. Comparing the Figure 5.2 with in Figure 4.11, the measured efficiency for the smaller vane antenna (#2) is slightly lower than that of antenna #1 in the first waveguide.
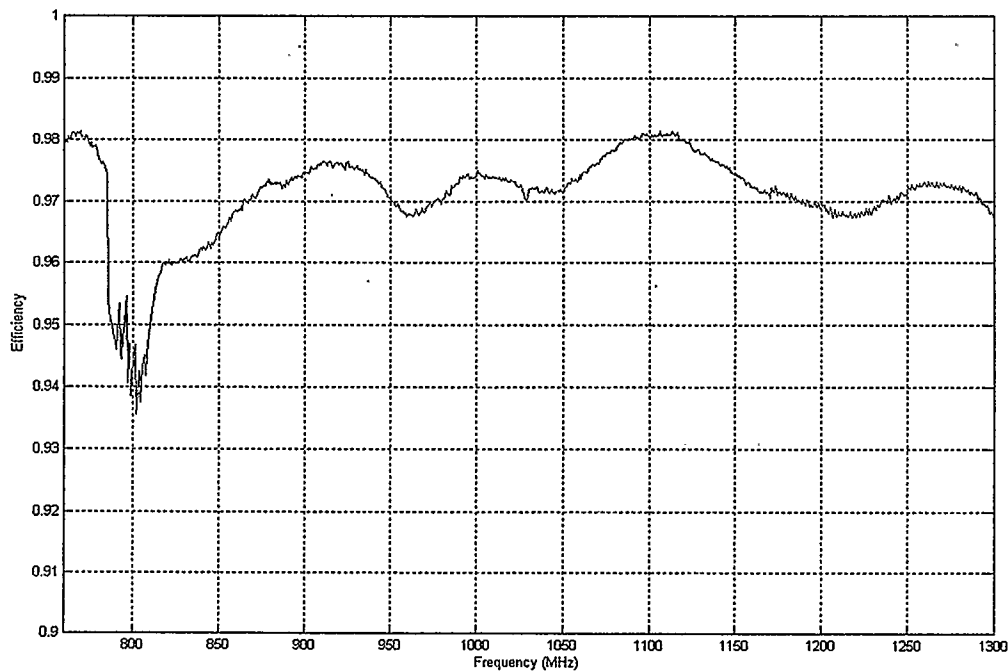

Figure 5.2 The measured efficiency of the vane antenna #2 in the precision waveguide

5.2.2 The monopole antenna

Three quarter wave monopoles with different diameters are measured. The results

on Figure 5.3 show that the larger diameter wires tend to have a measurably higher
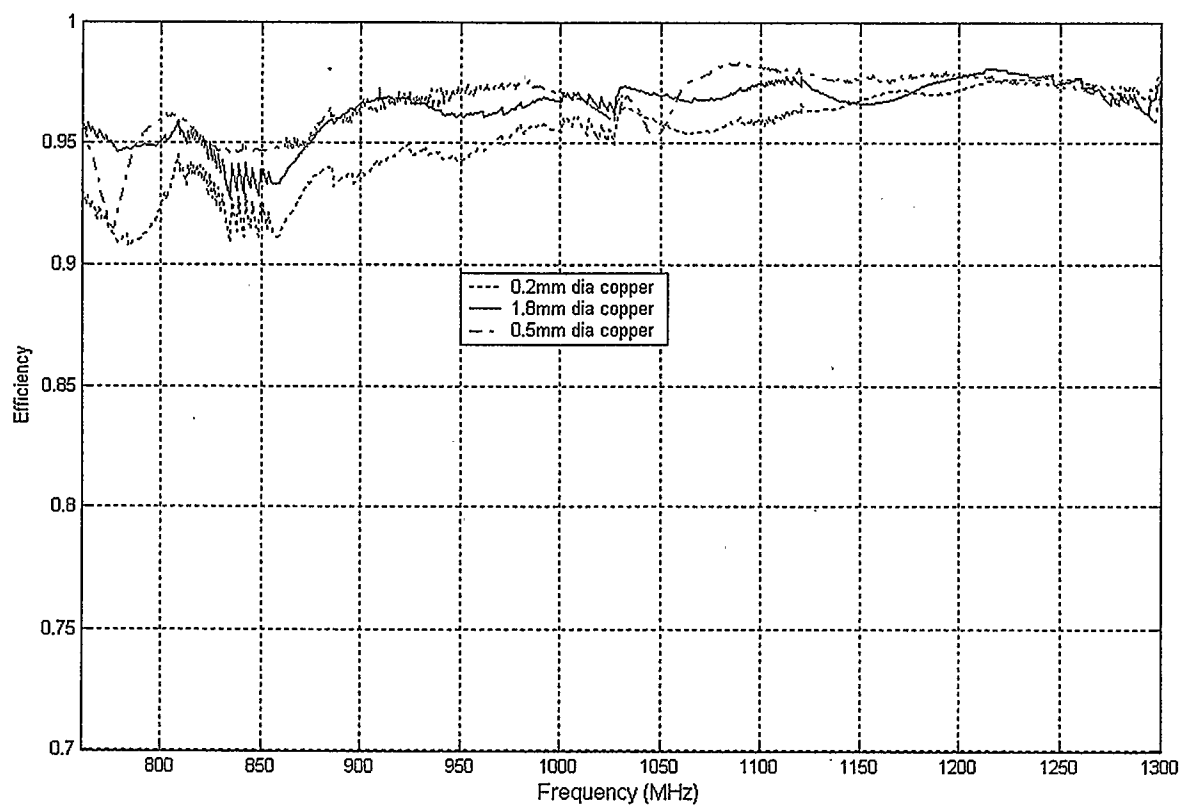
efficiency.

Figure 5.3 The efficiency of monopole antennas

5.3 Multimode measurement results

When the operation frequency is above 1.5 GHz, multimode waves are generated. According to the dimensions of the precision waveguide, the frequencies of multimode waves are 1.5 GHz, 1.677 GHz, 2.12 GHz, 2.25 GHz and 2.7 GHz etc. The vane antenna #2 is then measured from 1.3 GHz to 2.7 GHz to observe the multimode losses that affect the measured efficiency. Figure 5.4 and Figure 5.5 show the efficiency at the frequency range of 1.3 GHz to 2 GHz and 2 GHz to 2.7 GHz respectively. The efficiency notches in both figures are believed to be caused by multimode losses.
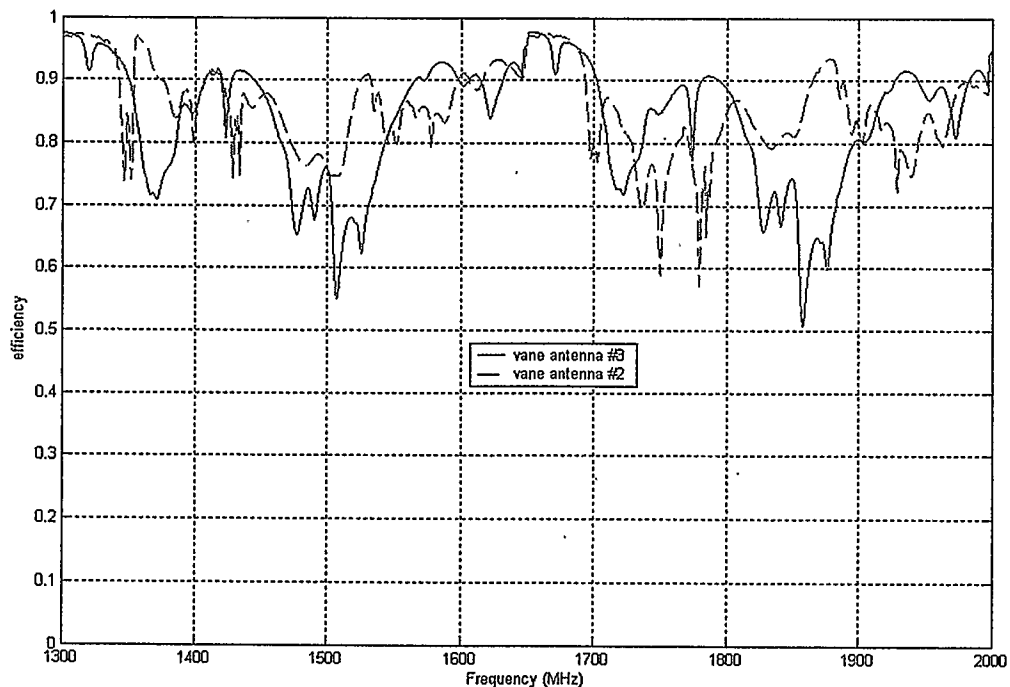

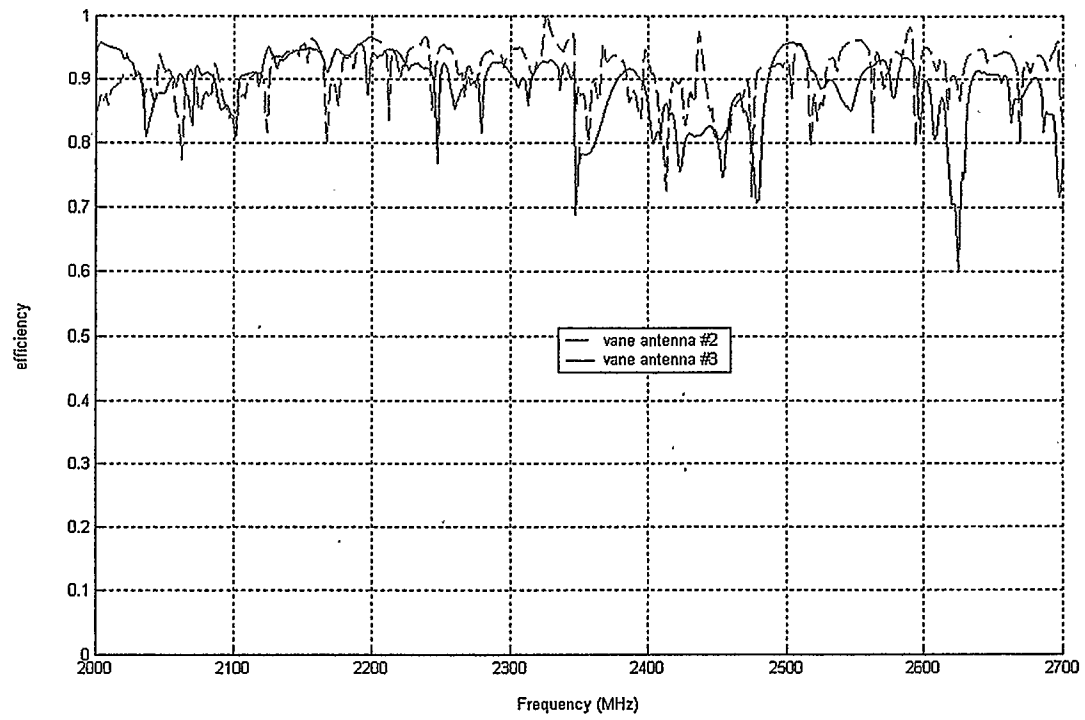Figure 5.4 Measured vane antenna #2 and 3 efficiency from 1.3 to 2GHz

Figure 5.5 Measured vane antenna #2 and 3 efficiency at from 2 to 2.7GHz

Chapter 6

Antenna Efficiency Measurement Using a Cubic Cavity

A cubic cavity with a mode stirrer was designed to measure the antenna efficiency based on the reflection method. Figure 6.1 shows the construction of the cubic cavity. The construction and use of this structure is original to this research project.
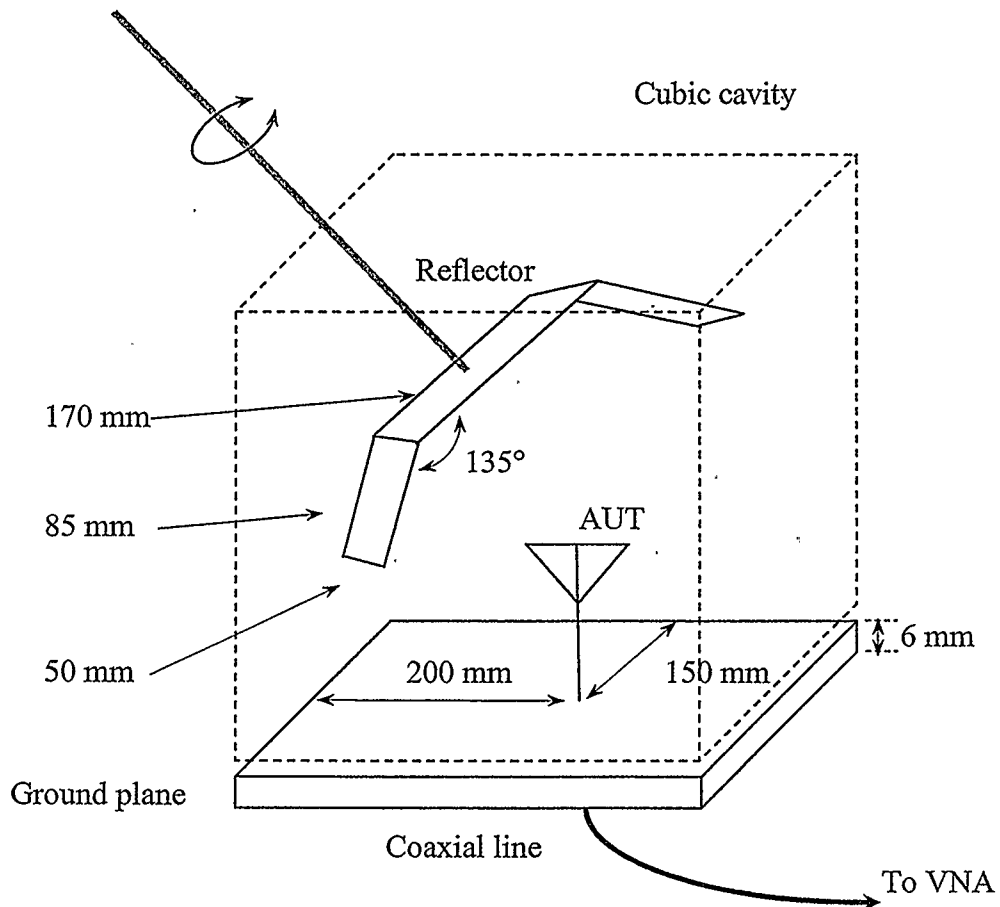

Figure 6.1 Efficiency measurement using a cubic cavity

6.1 Construction of the cubic cavity

The inside dimension of the cubic cavity is 304×304×302 mm. Other dimensions are shown in Figure 6.1.The upper part of the cavity overlaps the ground plane and is compressed against the ground plane with screws spaced by 38mm. The rotatable conductive reflector (or mode stirrer) serves the same purpose as the sliding short in the waveguide which is to vary the reactance seen by the antenna output. When one rotates the mode stirrer, S_{11wg} describes a circle on the Smith chart.

6.2 Measurement of vane antennas in the cubic cavity

The measurements were carried out in the frequency range of 800 MHz to 3000 MHz, which is much wider than the measurement in the waveguide. The AUTs are still the same vane antennas. The measurement procedure is similar to the measurements in the waveguide. To obtain a good definition of the circle, 20 S_{11wg} values were measured at 20 different angular positions of the mode stirrer. Figures 6.2-6.4 indicate the measurement result for three vane antennas shown in Figure 4.10.
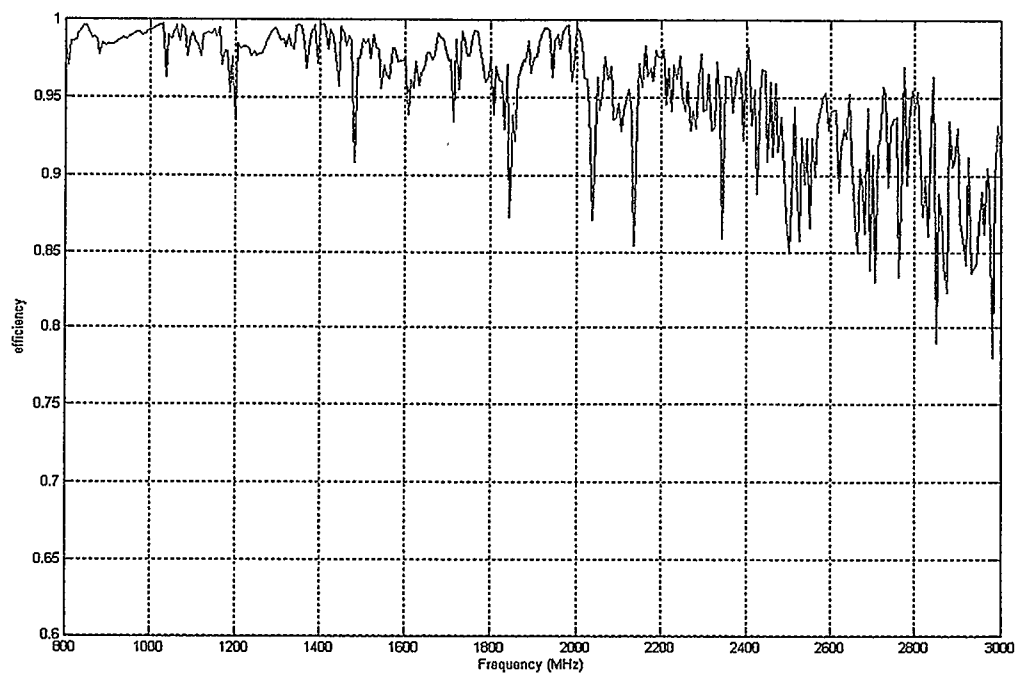
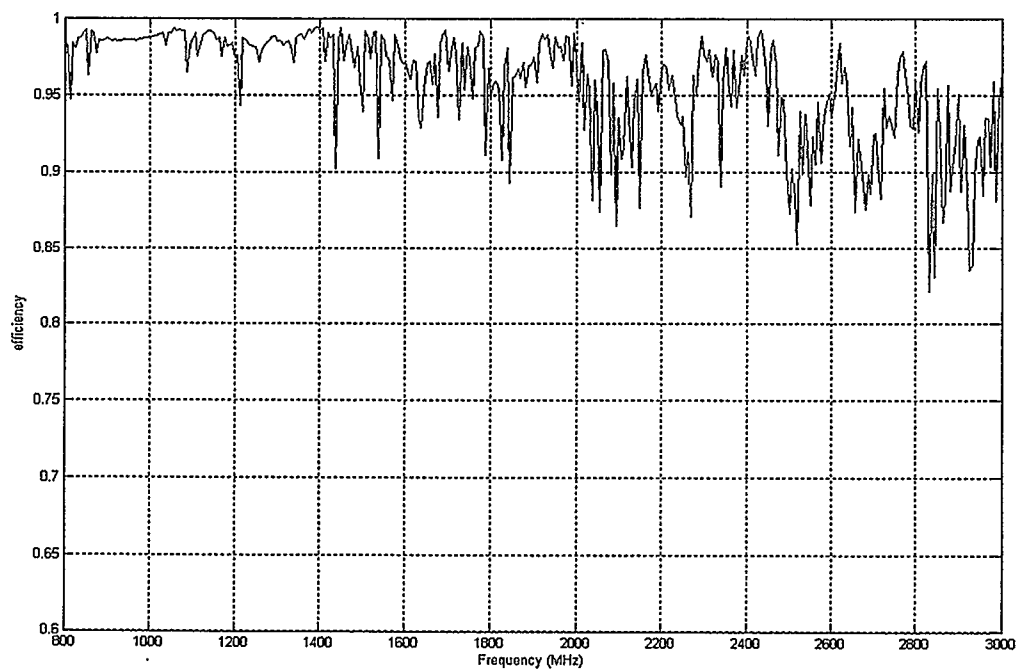Figure 6.2 The measured efficiency of vane antennas #1 in a cubic cavity

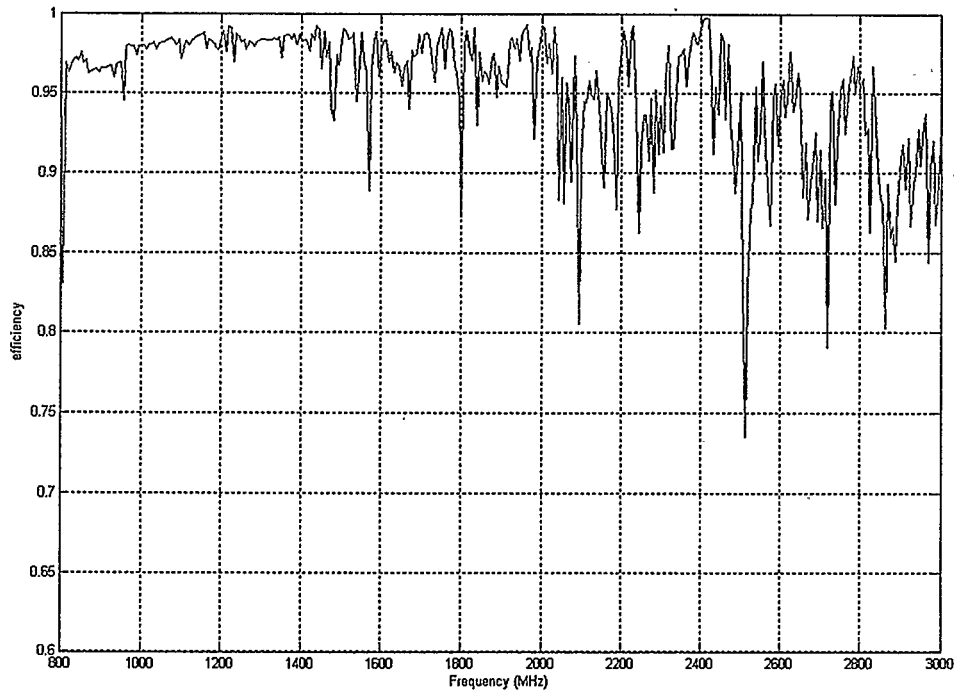Figure 6.3 The measured efficiency of vane antennas #2 in a cubic cavity

Figure 6.4 The measured efficiency of vane antennas #3 in a cubic cavity

It can be seen that the cubic cavity gives a better frequency range for accurate measurements than the over moded waveguide by comparing Figure 6.2 with Figure 4.11. However, the multimode losses will still introduce efficiency notches. According to the dimensions of the cubic cavity, the notches may occur at the frequencies of about 700, 1000, 1082, 1400 MHz and with increasing frequency, the notches begin to occur almost as a continuum. In both the waveguide and the cubic cavity, non ideal construction will affect the cutoff frequencies of the higher modes. Not all higher order modes will be activated by the antenna and in such cases efficiency notches will not be observed.

The rotatable "mode stirrer" does not suffer the problem of the small twist of the sliding short in the waveguide. It may be seen that the rotatable "mode stirrer" proved to

be quite effective in providing a variable reactance cavity to enclose the antenna. This has allowed the antenna efficiency to be measured over a wide frequency range.

6.3 Measurement of different wire monopole antennas

Three different diameters of monopoles in Section 4.5.2 were then measured in the cubic cavity in the frequency range from 750 MHz to 1000 MHz. Figure 6.5 shows the result. For each frequency, 24 S_{11wg} were measured instead of 10.
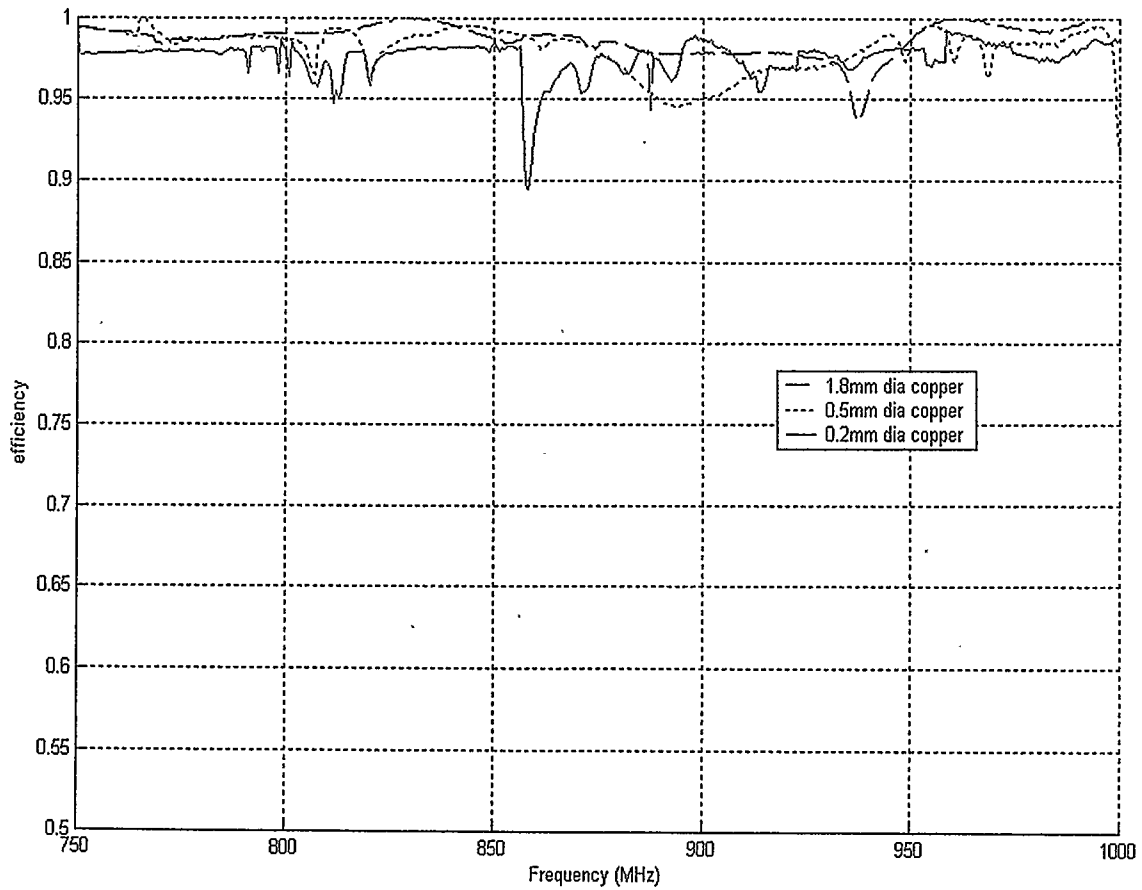

Figure 6.5 The efficiencies of different wire monopoles measured in the cubic cavity

6.4 Measurement of the reference loss antenna in the cubic cavity

A reference loss antenna can be built by connecting an attenuator in cascade with the reference antenna described in section 4.4. The efficiency of the overall antenna may be calculated, using the measured S parameters of the attenuator and $S_{11,fs}$ of the antenna. The structure is shown as in Figure 6.6.
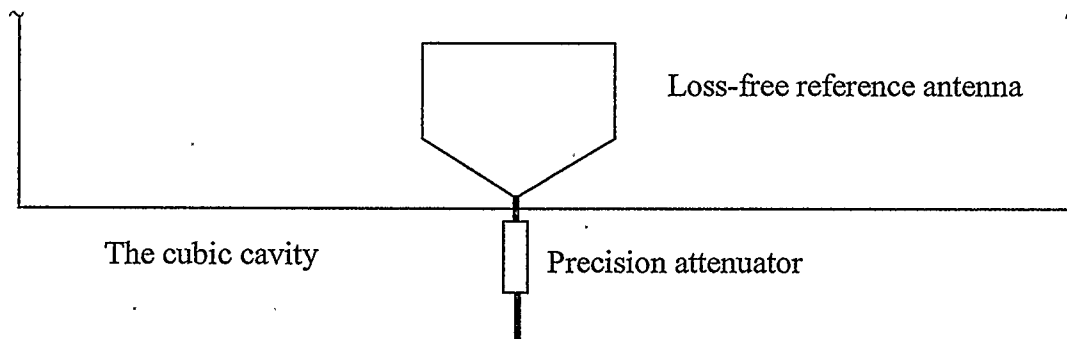

Figure 6.6 The construction of the reference-loss antenna

The measurements were taken in the cubic cavity. The attenuator was placed outside the cubic cavity connected in cascade with the reference antenna. 3 dB and 6 dB precision attenuators were used. Since the reference antenna has almost 100% efficiency, the reference-loss antennas with 3 dB and 6 dB are expected to have almost 50% and 25% efficiencies respectively. Figures 6.7-6.9 show the measurement results.
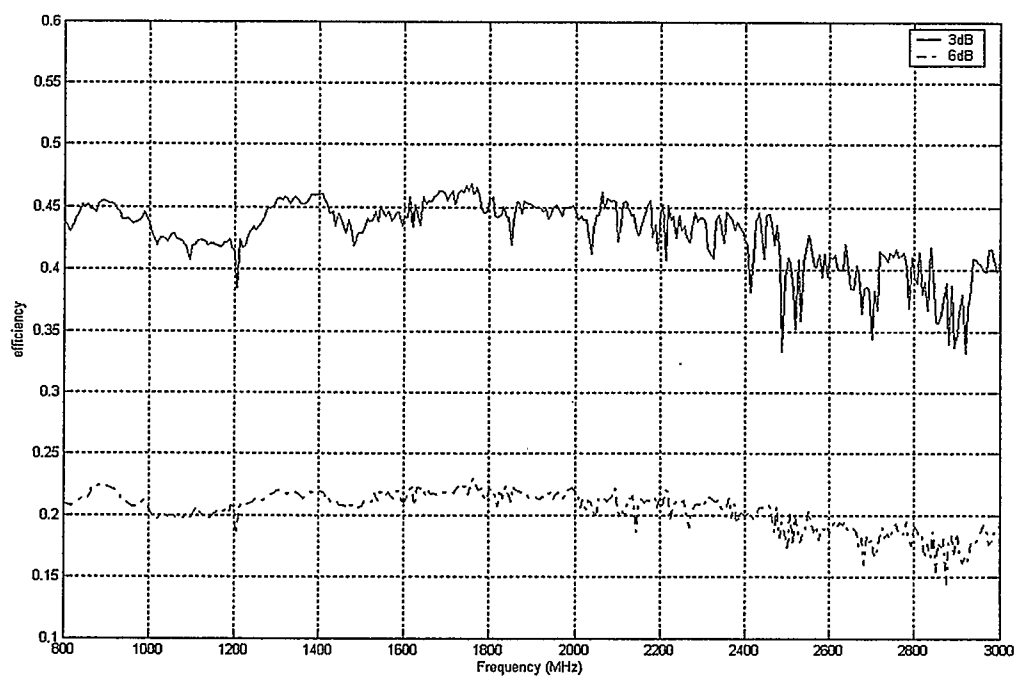
Figure 6.7 The efficiency of the vane antenna #1 with 3 dB and 6 dB attenuators
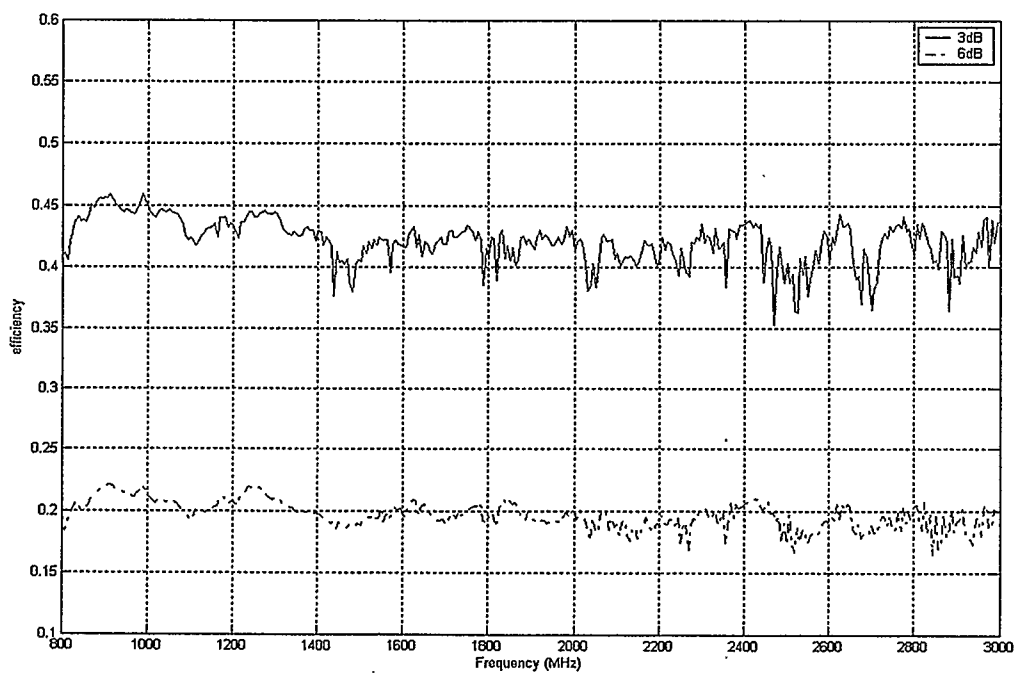

Figure 6.8 The efficiency of the vane antenna #2 with 3 dB and 6 dB attenuators
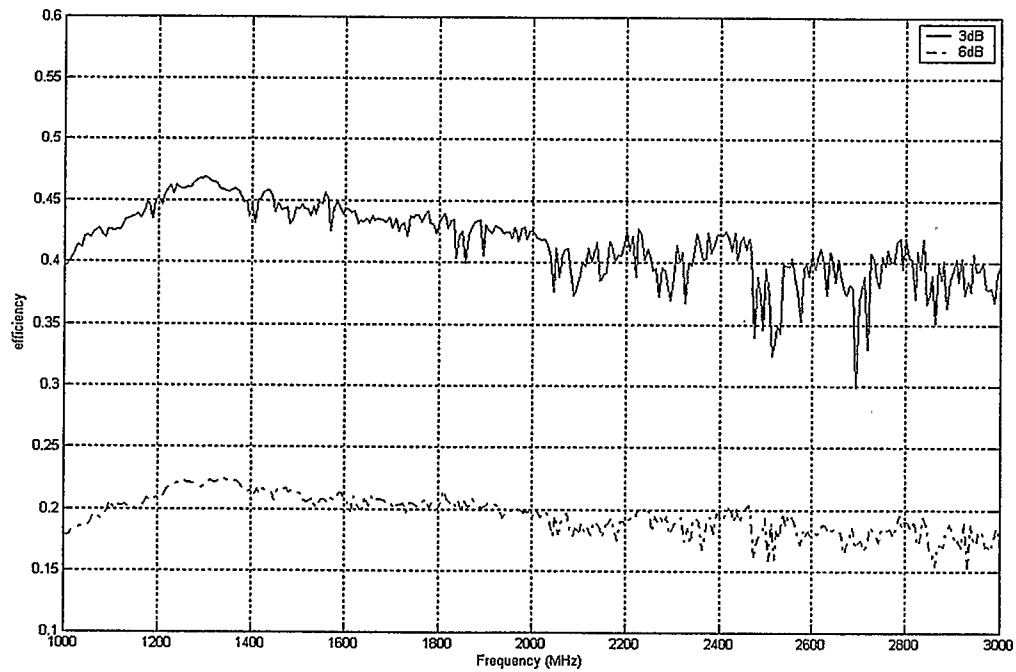
Figure 6.9 The efficiency of the vane antenna #3 with 3 dB and 6 dB attenuators

The efficiency of the reference-loss antenna can also be calculated. The construction of the reference-loss antenna may be modeled using the signal flow diagram as shown in Figure 6.10.
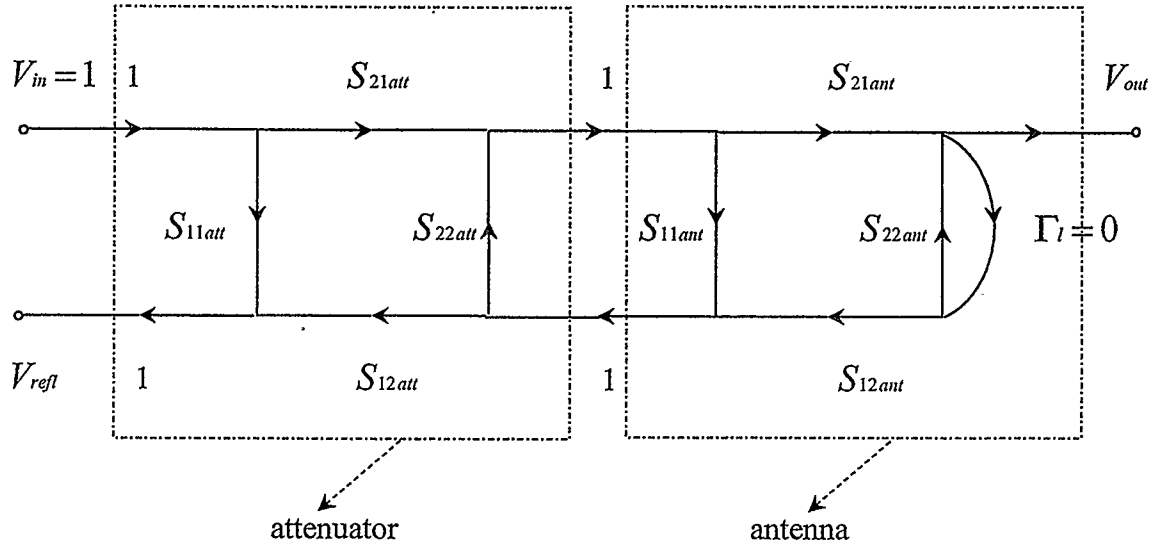
Figure 6.10 The equivalent signal flow diagram of the reference-loss antenna

Suppose the input voltage $V_{in} = 1$, then output voltage V_{out} and reflected V_{refl}

can be written directly by applying Mason's law :

$$V_{out} = \frac{S_{21att}S_{21ant}}{1 - S_{11ant}S_{22att}},$$

(6-1)

$$V_{refl} = \frac{S_{11att}(1 - S_{11ant}S_{22att}) + S_{21att}S_{11ant}S_{12at}}{1 - S_{11ant}S_{22att}} = S_{11att} + \frac{S_{21att}S_{11ant}S_{12att}}{1 - S_{11ant}S_{22att}},$$

(6-2)

where:

S_{11ant} = the S_{11} of antenna in free space,

S_{21ant} = the S_{21} of antenna,

$S_{11att}, S_{12att}, S_{21att}$ and S_{22at} = the S parameters of the attenuator.

The efficiency can be expressed as :

$$\eta = \frac{|V_{out}|^2}{1 - |V_{refl}|^2} .$$

(6-3)

Substitute (6-1) and (6-2) into (6-3) yields:

$$\eta = \frac{\left| \dfrac{S_{21att}S_{21ant}}{1 - S_{11ant}S_{22att}} \right|^2}{1 - \left| S_{11att} + \dfrac{S_{21att}S_{11ant}S_{12att}}{1 - S_{11ant}S_{22att}} \right|^2} .$$

(6-4)

To calculate the efficiency, the S-parameter of the attenuator and the S_{11ant} need to be directly measured and the S_{21ant} can be found from the measurement without attenuator attached. The calculation and the measurement results are both plotted in the same figures for the purpose of comparison.

Figure 6.11 to 6.16 are the results of measurements and calculations. The results generally show good agreement with each other.
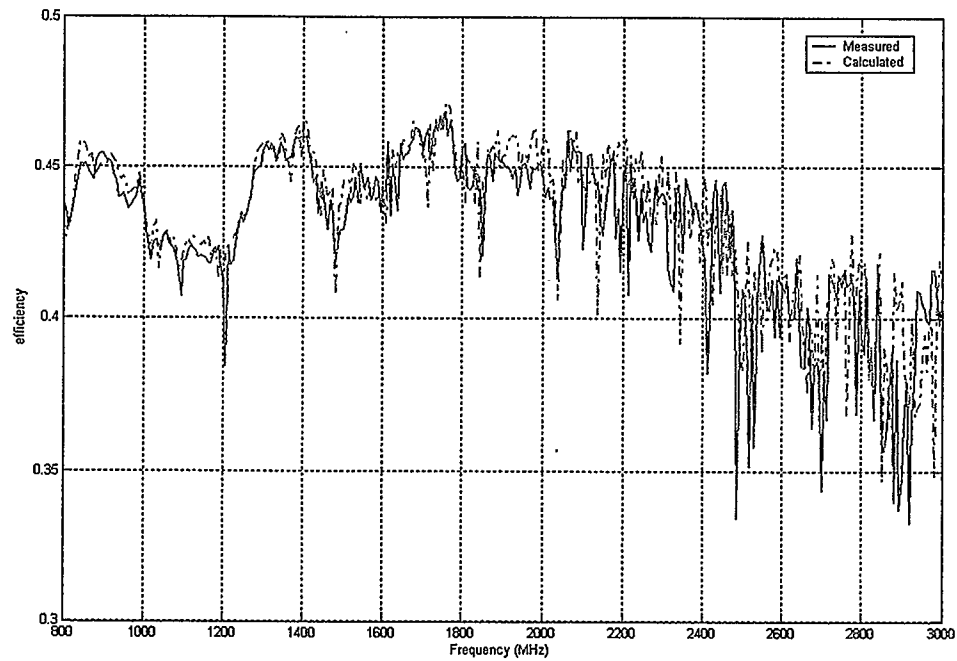
Figure 6.11 The calculated and measured efficiency of the vane antenna #1 with a precision 3 dB attenuator
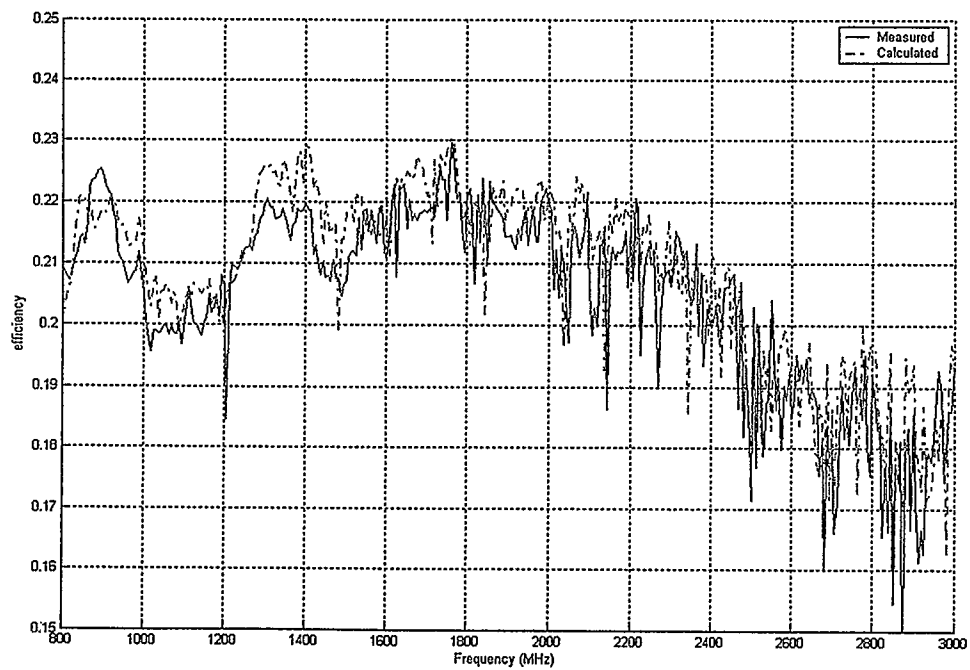

Figure 6.12 The calculated and measured efficiency of the vane antenna #1 with a precision 6 dB attenuator

Figure 6.13 The calculated and measured efficiency of the vane antenna #2 with a precision 3 dB attenuator

Figure 6.14 The calculated and measured efficiency of the vane antenna #2 with a precision 6 dB attenuator
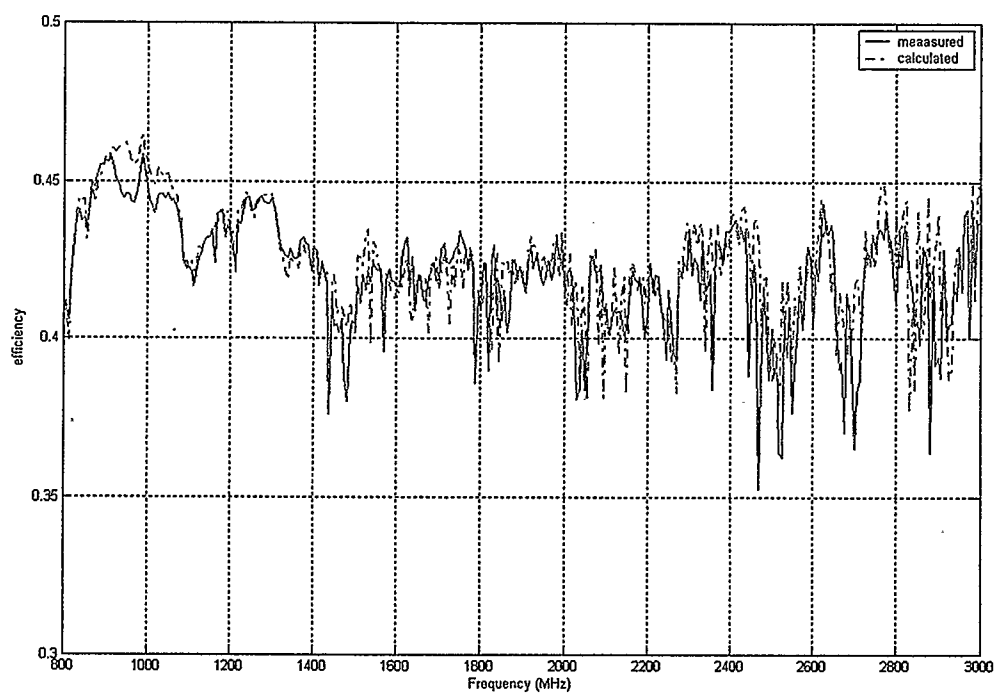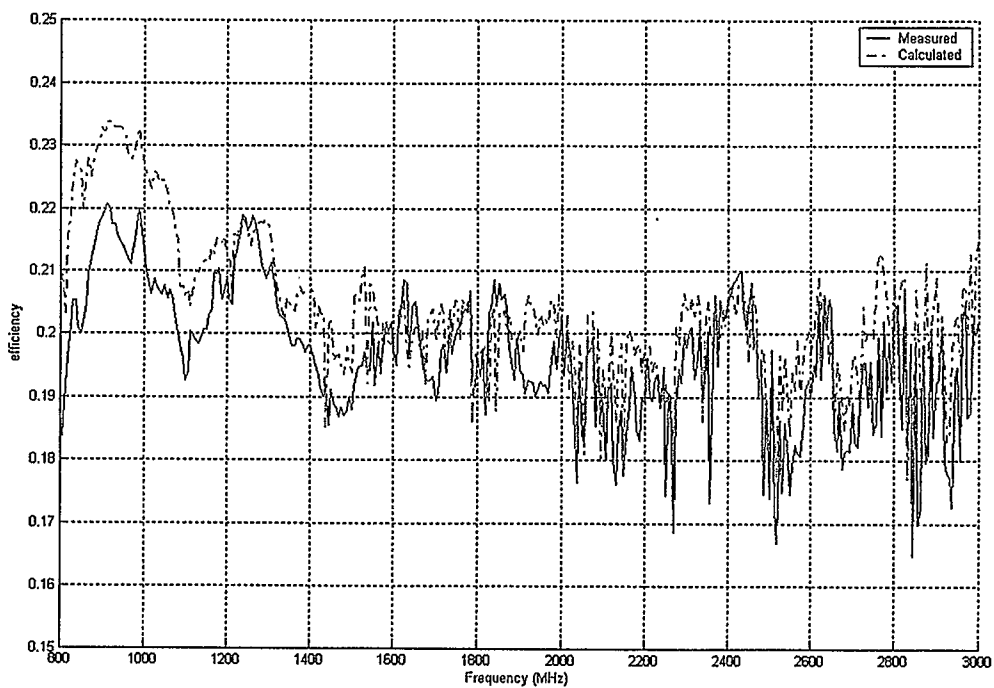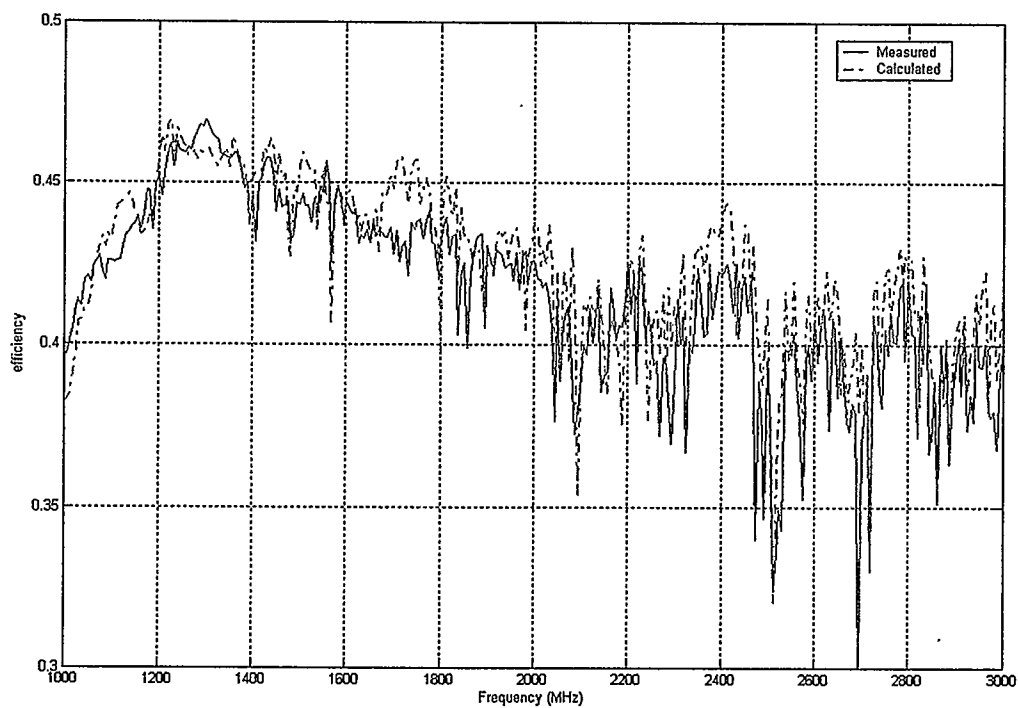
Figure 6.15 The calculated and measured efficiency of the vane antenna #3 with a
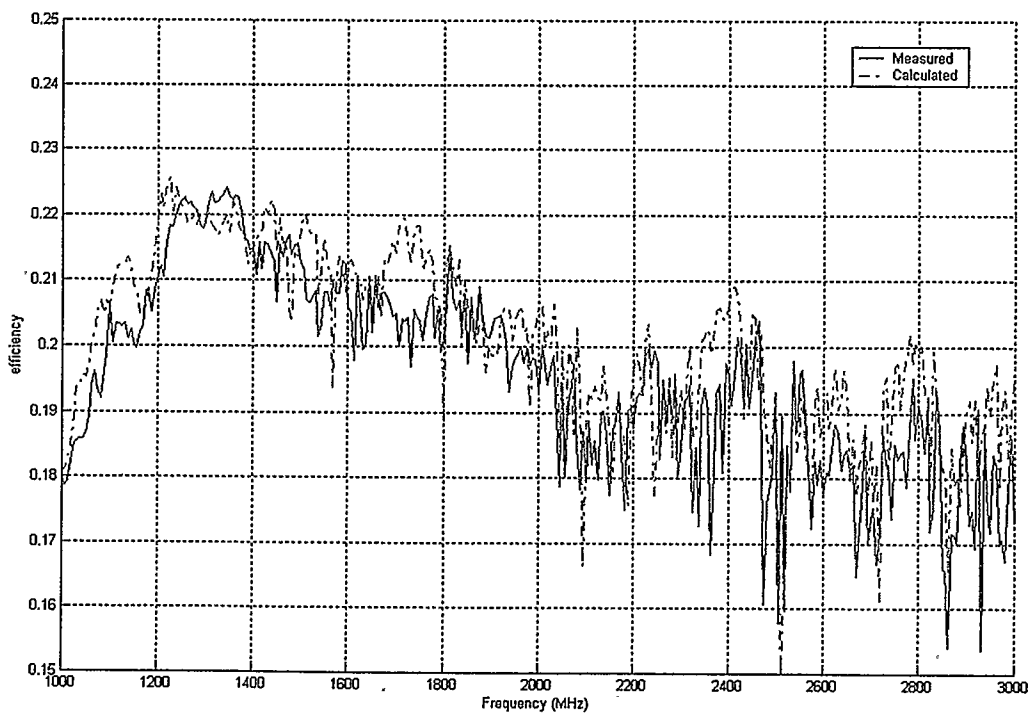precision 3 dB attenuator

Figure 6.16 The calculated and measured efficiency of the vane antenna #3 with a
precision 6 dB attenuator

6.5 Measurement of a microstrip patch antenna

The compact microstrip patch antenna now finds many applications in modern PCS and other wireless services. To improve the bandwidth, a low-value resistance can be used to replace the short-circuit in a standard quarter-wave patch antenna [10]. The structure of the quarter-wave microstrip patch antenna with resistive loading is shown in Figure 6.17.

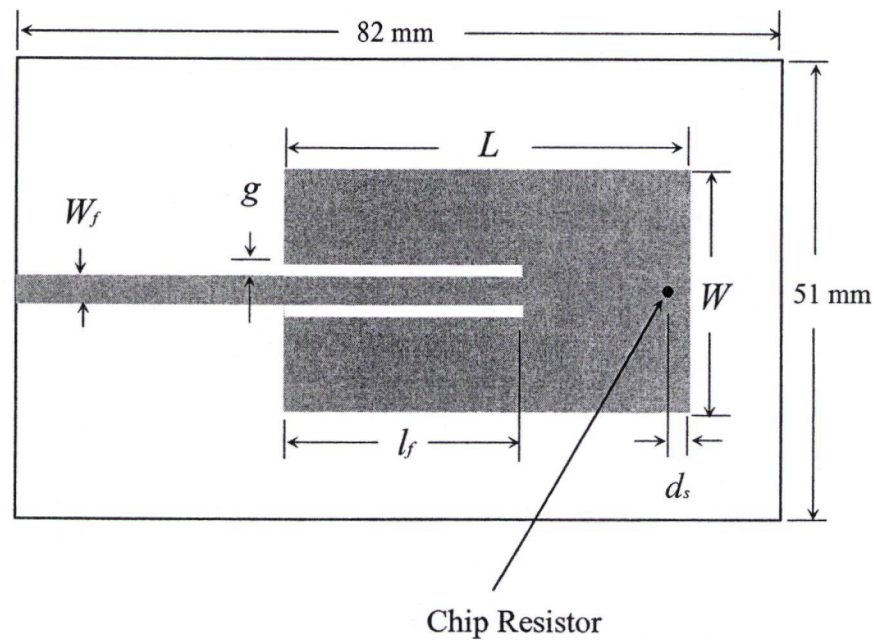Figure 6.17 The structure of a resistively-loaded microstrip patch

The experimental antenna was built on a 1.524mm substrate with $\varepsilon_r = 3.05$ and $\tan \delta = 0.003$. The substrate measured 82mm by 51mm, and the patch had the following

dimensions: L=40.6 mm, W=25 mm, lf=32.4 mm, ds =2.2 mm, Wf=3.5 mm, and g =1.65 mm. The microstrip patch antenna can be treated as microstrip transmission line resonator with appropriate resistive loads terminating the line. For a quarter-wave patch antenna, one end of the resonant transmission line is connected to the substrate ground plane by a short or a low value resistor, as shown in Figure 6.18. The feed line input is 50 Ω as calculated by the dimensions of the antenna shown in Figure 6.17.
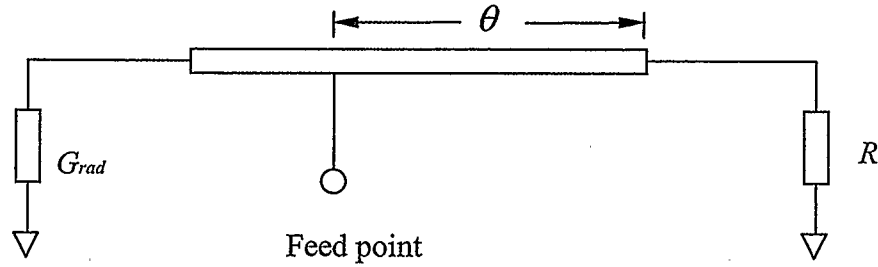

Figure 6.18 The equivalent circuit of the quarter-wave resistively-loaded patch

In Figure 6.18, G_{rad} is the radiation conductance at the open end of the resonator and R is the value of the resistive load. The G_{rad} and R may be transferred to the feed point using [11]:

$$G_{frad} = \frac{G_{rad}}{\sin^2 \theta},$$
(6-5)

$$G_{fpres} = \frac{R}{Z_o^2 \sin^2 \theta},$$
(6-6)

where: Z_0 = the effective characteristic impedance of the microstrip line

resonator,

G_{ffrad} = the conductance at the feed point transferred from the radiation

conductance,

G_{ffpres} = the conductance at the feed point transferred from load resistance.

· The efficiency of the antenna can be calculated as:

$$\eta = \frac{G_{ffprad}}{G_{ffpres} + G_{ffprad}} = \frac{Z_0^2 G_{rad}}{Z_0^2 G_{rad} + R}, \tag{6-7}$$

In [10], G_{rad} can be expressed by:

$$G_{rad} = \frac{4\pi h W_e}{3\lambda_0^2 \sqrt{\varepsilon_{eff}}}, \tag{6-8}$$

where:

W_e = the effective width of the resonator,

ε_{eff} = the effective dielectric constant of the microstrip antenna,

h = the substrate height,

λ_0 = the wavelength in free space.

For the antenna structure shown in Figure 6.17, equation (6-7) gives an efficiency of 0.96%, which is approximate as many simplifying assumptions have been made. For instance, current crowding and capacitive effect are not accounted for. In [10], two numerical simulation techniques were used to evaluate the performance of the antenna structure shown in Figure 6.17. One simulation used the moment method

(software package known as WIPL-D) to compute relevant antenna parameters while the other used the FDTD technique. The WIPL-D simulation was found to have an efficiency of 0.41% while the FDTD yielded an efficiency of 0.76%.

The efficiency of the experimental antenna terminated by 1Ω was then measured in the rectangular waveguide at its resonant frequency of 830 MHz with a 24 dB return loss. The S_{11wg} of the antenna was measured with 10 different positions of the sliding short. The Figure 6.19 shows the 10 measured S_{11wg} pointed as "*" plotted on the polar coordinate system. The "+" represents the measured S_{11fs}. The solid line is the circle that fits to the 10 measured S_{11wg} points. The measured result is 3% which is higher than that predicted by numerical moment and FDTD methods. In the laboratory measurements of the antenna, the feedline could have been contributing to the radiation which can result in a higher efficiency than that exhibited by the antenna itself. Another issue is that the S_{11fs} is very close to the fitted circle. This yields a very small value of ΔS_{min}. From equation (4-33), a very small ΔS_{min} will make the efficiency very small as well as degrading the measurement accuracy. S. Hum and M. Okoniewski were responsible for the antenna construction and FDTD analysis while R. Johnston provided the algebraic efficiency calculation and the WIPL efficiency determination.
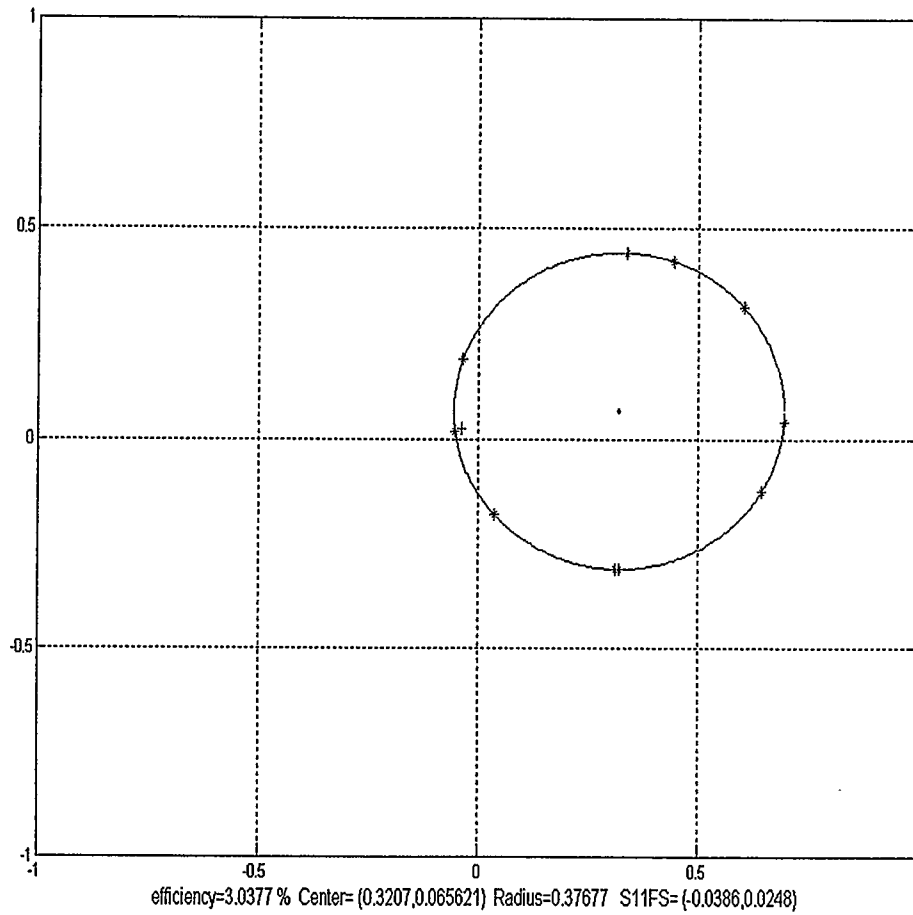
efficiency=3.0377 % Center= (0.3207,0.065621) Radius=0.37677 S11FS= (-0.0386,0.0248)

Figure 6.19 The polar plot of the S_{11wg} (*), the fitted circle and S_{11fs} (+)

6.6 Measurement of a resistively-loaded microstrip patch antenna

The quarter-wave resistively-loaded patch possesses a very low overall efficiency because the resistor is introduced at the point where large current flow exists, maximizing the effect of the resistance. A novel patch antenna [12] developed by S.Hum and M. Okoniewski in our institution is shown in Figure 6.20. The resistor was installed at the

points where current density is less. The efficiency will then be improved while still taking advantage of resistors to broaden the bandwidth. Grounding of the patch was achieved through the use of N regularly spaced vias placed along both edges of the antenna. Adjusting the slot length and resistor value allows the amount of current flowing through the resistor and hence the bandwidth/efficiency characteristic offered by the antenna to be controlled. The antenna was fabricated on a 1.524mm $\varepsilon_r = 3.2$ microwave substrate with the following parameters: $F = 6.5mm, L = 38mm, W = 40mm, S = 12mm,$ $O = 10mm$ and $N = 12$.
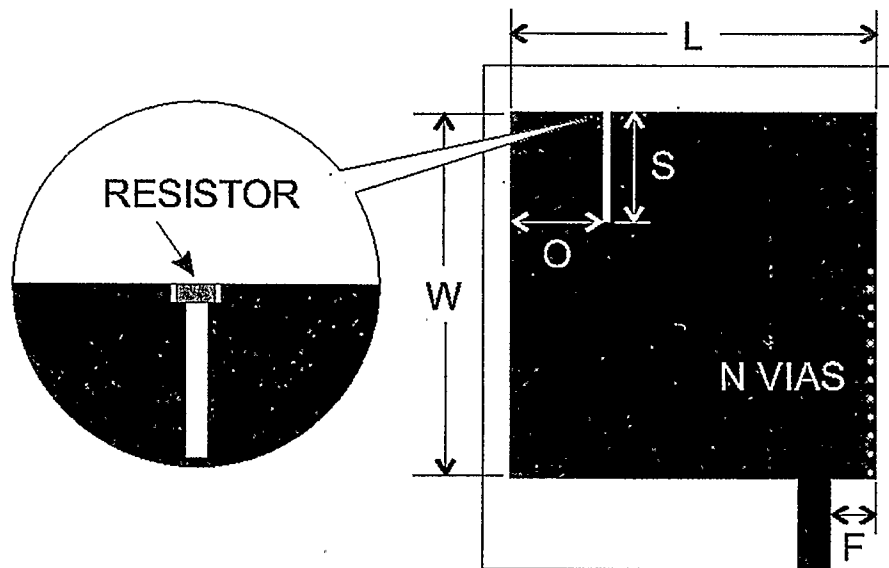

Figure 6.20 Layout of a novel resistively-loaded patch antenna with controllable bandwidth

The bandwidth and efficiency of this antenna was measured experimentally as the load resistance was discretely varied over a $1-1000\Omega$ range at the resonant frequency.

Both bandwidth and efficiency are plotted in Figure 6.21. As expected, the trend is that

higher bandwidths with corresponding the lower efficiencies are obtained. At $R = 39 \ \Omega$,

the bandwidth of the antenna is maximized at 1.3% while the efficiency is minimum at

approximately 26%. Clearly, the bandwidth and efficiency exhibited by the antenna can
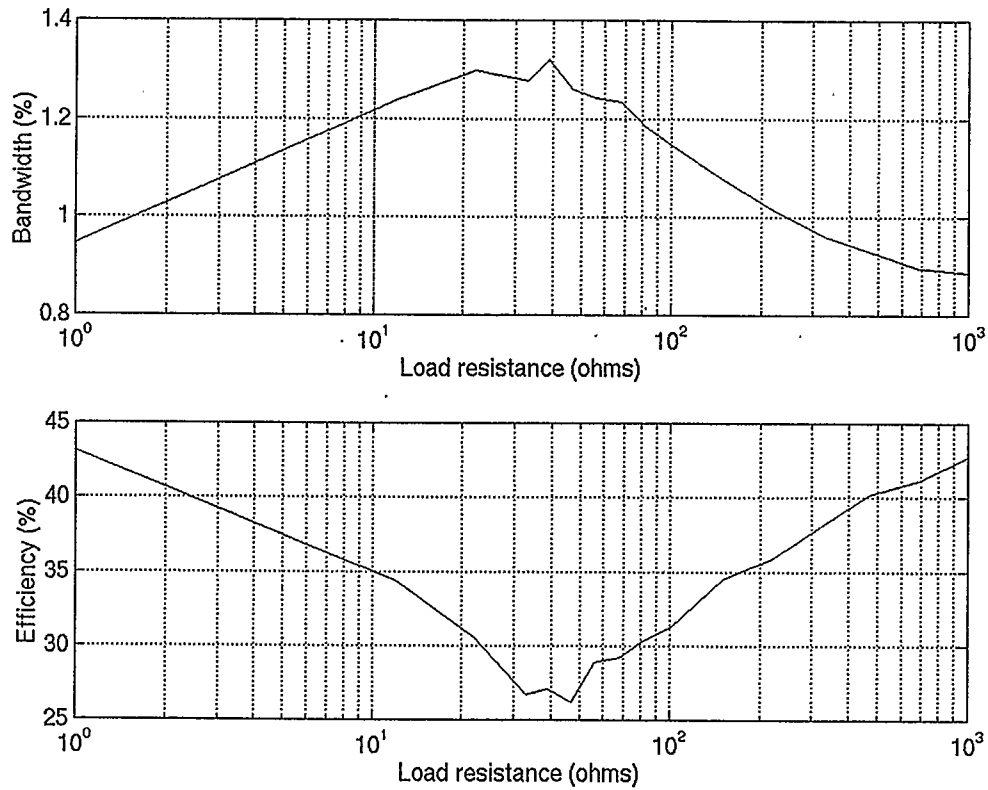
be controlled by adjusting the load resistance.

Figure 6.21 Measured antenna bandwidth and efficiency versus slot load resistance

Again, examining the Figure 6.24 shows the 10 measured S_{11wg}, the fitted circle and the

S_{11fs} at $R = 10\Omega$. The measured efficiency is 35% which is much higher than the

resistively-loaded quarter-wave patch antenna as presented in 6.5. By comparing Figure

6.22 and 6.19, the higher efficiency results from not only the larger radius of the fitting

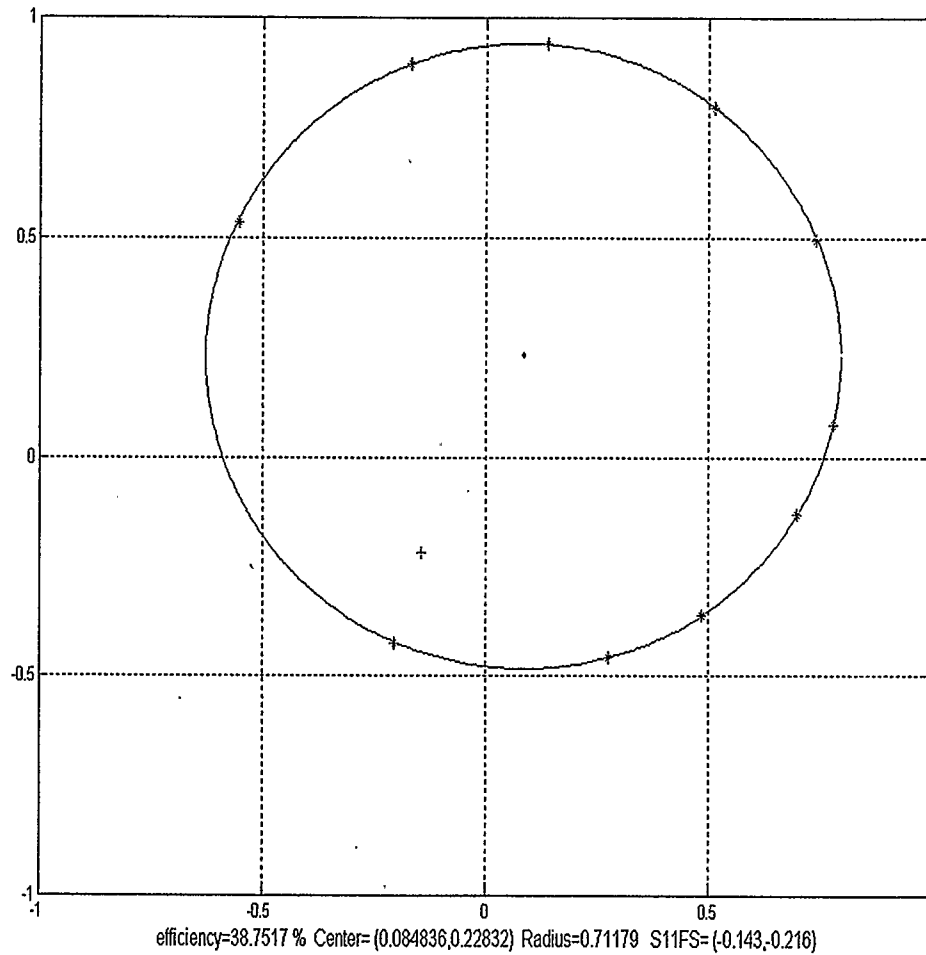circle, but also the longer distance between the edge of the circle and the S_{11fs}.

efficiency=38.7517 % Center= (0.084836,0.22832) Radius=0.71179 S11FS=(-0.143,-0.216)

Figure 6.22 The polar plot of the S_{11wg} (*) , the fitted circle and S_{11fs} (+)

Chapter 7

Removal of ill-conditioned data

As we mentioned in previous chapter, when we rotate the mode stirrer or the sliding short, 10 to 20 measured S_{11wg} will be used to determine the circle. If we need to measure the efficiency only at a certain frequency, e.g. the patch antenna in section 6.6, we can observe the rotating S_{11wg} on the VNA and try to adjust the mode stirrer or sliding short to have optimum 10-20 positions to ensure the measured S_{11wg} evenly distributed in order to obtain high accurate circle definition. However, if we need to measure the antenna efficiency over a wide frequency range, the measured S_{11wg} can not be observed on VNA at each frequency.

7.1 Removal of S_{11wg} data on a limited arc

The rotating of S_{11wg} is not linearly proportional to the rotating of the mode stirrer or sliding short. A large rotation of the mode stirrer may cause a tiny rotation of the S_{11wg} while at other angle a tiny rotation of the mode stirrer may cause a large rotation of the S_{11wg}. Therefore, the 10 to 20 measured S_{11wg} may concentrate in a very small arc which results in a badly defined circle. For example, consider the vane antenna #2 measurement in section 6.2, at a frequency of 1.9125 GHz as shown in Figure 7.1. All 20 measured S_{11wg} are close each other which increases the error of the circle definition. However, at a frequency of 1.8 GHz, as shown in Figure 7.2, 20 measured S_{11wg} are well distributed and can be used to define an accurate circle and efficiency calculation.
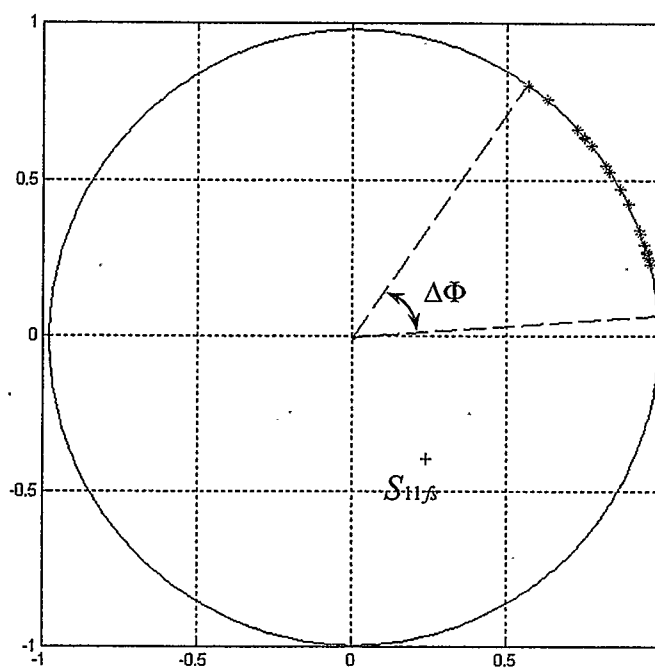
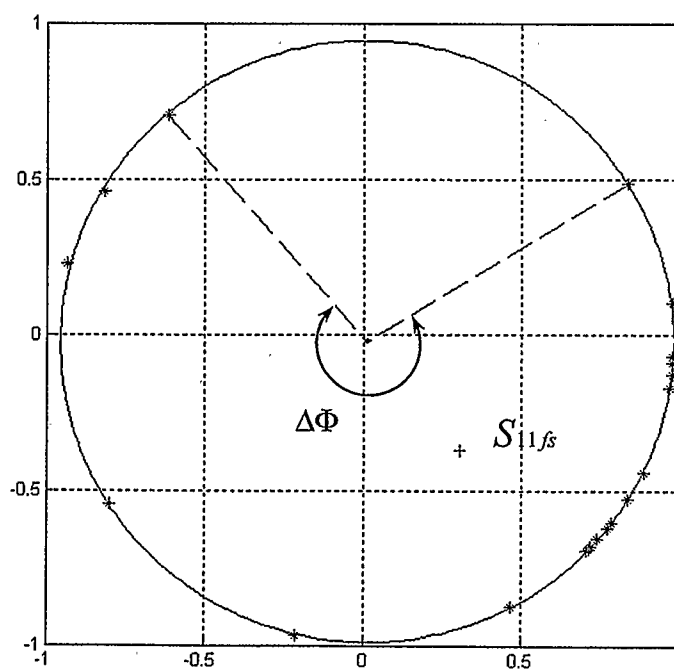Figure 7.1 An ill-defined circle

Figure 7.2 A well defined circle

This situation will still occur even if we take more than 20 measurements at each frequency. In both Figure 7.1 and 7.2, the $\Delta\Phi$ can be used to describe how well these measured S_{11wg} values are distributed. If we assume that when $\Delta\Phi > 90°$, the measured points can used to define the circle accurately. Otherwise, they can not be used to define circle and the efficiency at that frequency should be treated as "unknown". To measure that efficiency at these particular frequencies, we can set the VNA to that frequency only and observe the rotating S_{11wg} which is same method as we measured the previous patch antenna.

7.2 Removal of S_{11wg} data on a varying radius

By observing some circles at some frequencies, we found that at some frequencies, a few measured S_{11wg} obviously deviated from the circle. For example, the vane antenna #2 measurement in section 6.2, at a frequency of 2.99 GHz (refer to Figure 7.3), 3 measured S_{11wg} values are far away from the defined circle. This will lead to an inaccurately defined circle. To numerically describe the deviation, we use R_{cir} as the radius of the defined circle and R_n as the radius of the nth measured S_{11wg}. Then the deviation δ can be expressed as

$$\delta = \frac{1}{n}\sum_{n=1}^{n}\frac{|R_n - R_{cir}|}{R_{cir}} \qquad (7\text{-}1)$$

The deviation shown in Figure 7.3 is 0.02218. Practically, we set the threshold to 0.02, i.e., if $\delta > 0.02$, that set of S_{11wg} values cannot be used to define a circle and that efficiency at that frequency is unknown and should be measured separately.
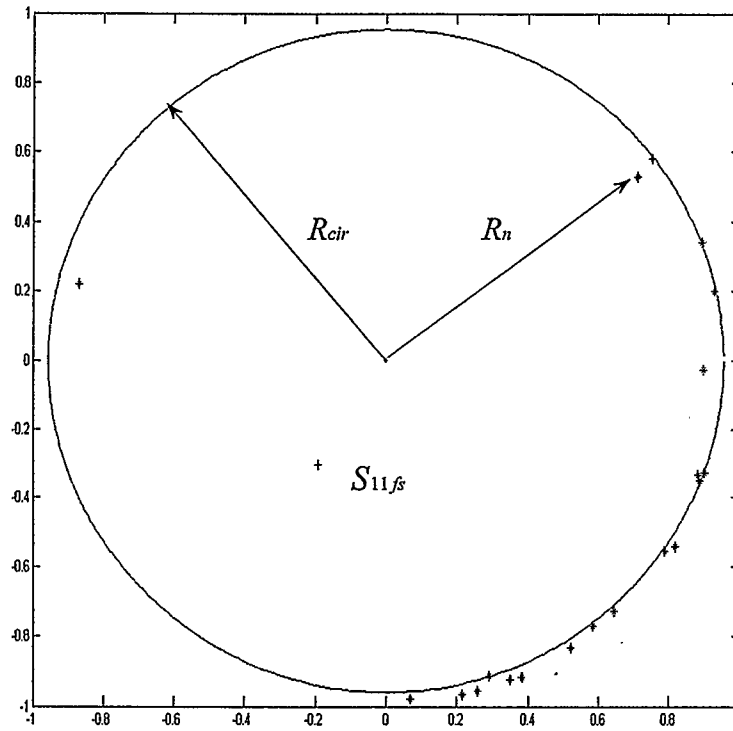

Figure 7.3 The deviation of S_{11wg}

7.3 Results

By incorporating above two criteria with MATLAB, the data measured can be re-processed. For vane antenna #2 measured in the cubic cavity, the result is shown in Figure 7.4. Because, the efficiency is unknown at some frequencies, the result is not

plotted as a continuous line. The black dots show the discrete efficiency values while the dotted line is the efficiency without applying the above two criteria.
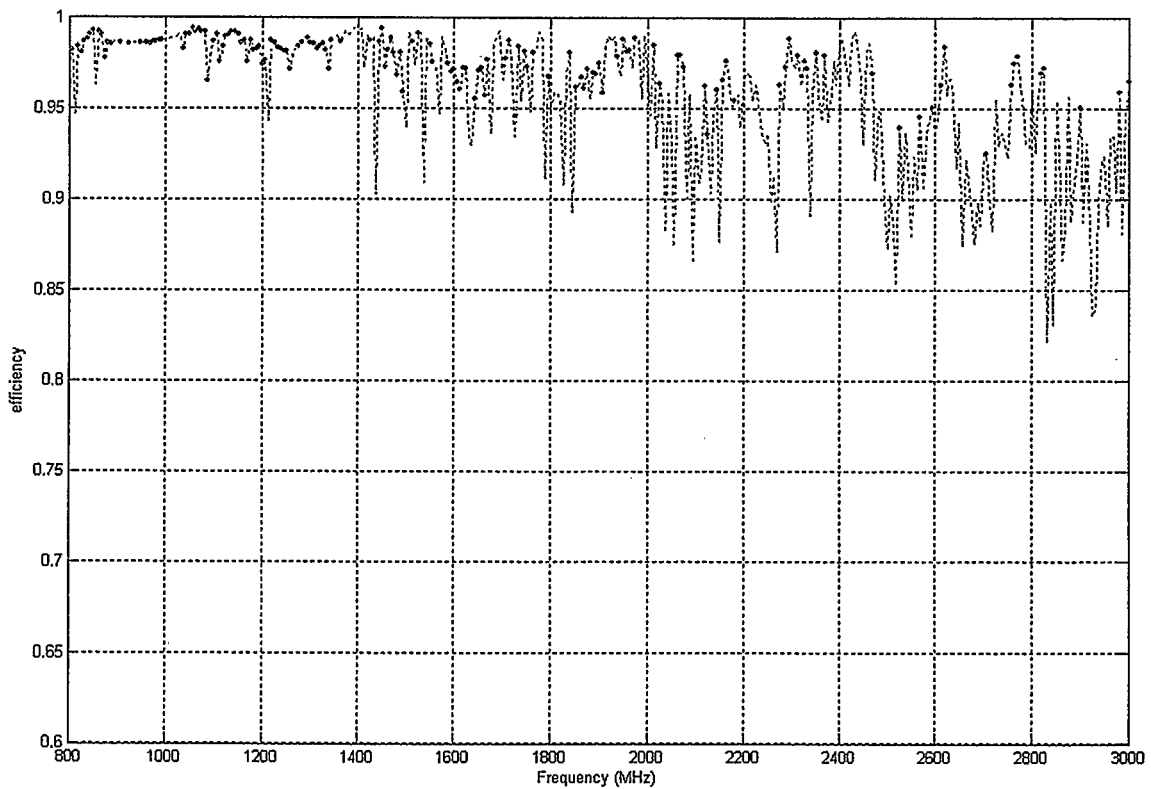

Figure 7.4 Measured vane antenna #2 in the cubic cavity with improved data process

The following Figures 7.5 to 7.10 are the re-processed results of three vane antennas cascaded with attenuators while the original results are shown in Figure 6.11 to 6.16. The approach of removing efficiency data points based on ill conditioned input data is original to this research.
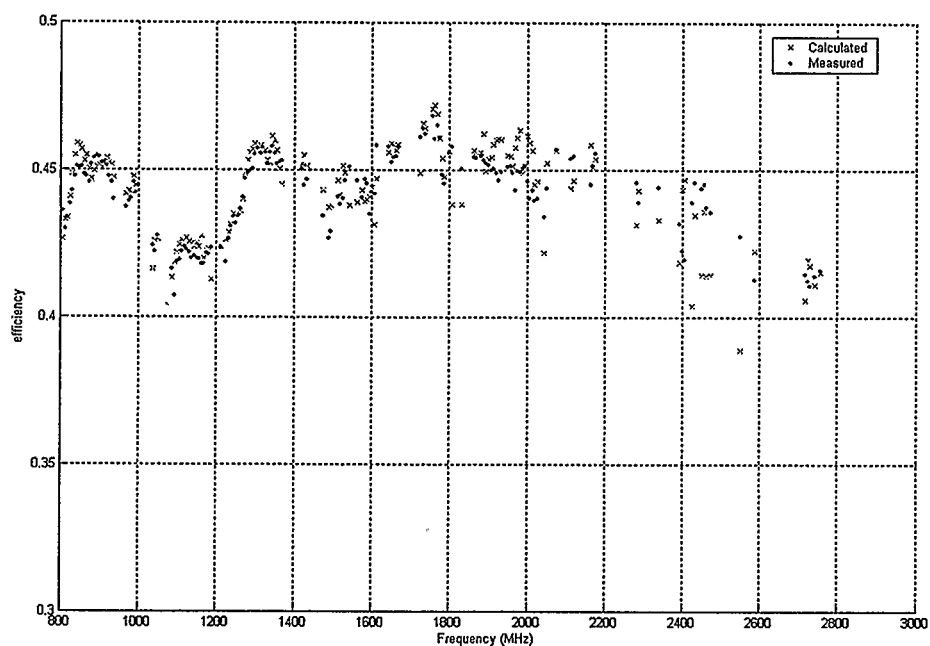
Figure 7.5 The calculated and measured efficiency of the vane antenna #1 with a precision 3 dB attenuator with improved data process
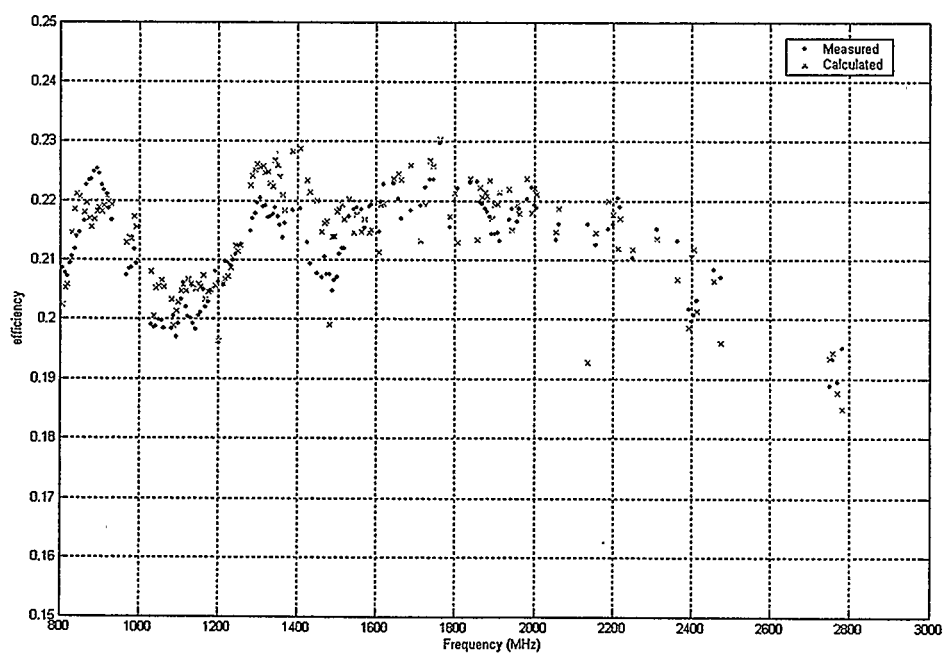

Figure 7.6 The calculated and measured efficiency of the vane antenna #1 with a precision 6 dB attenuator with improved data process

Figure 7.7 The calculated and measured efficiency of the vane antenna #2 with a precision 3 dB attenuator with improved data process

Figure 7.8 The calculated and measured efficiency of the vane antenna #2 with a precision 6 dB attenuator with improved data process
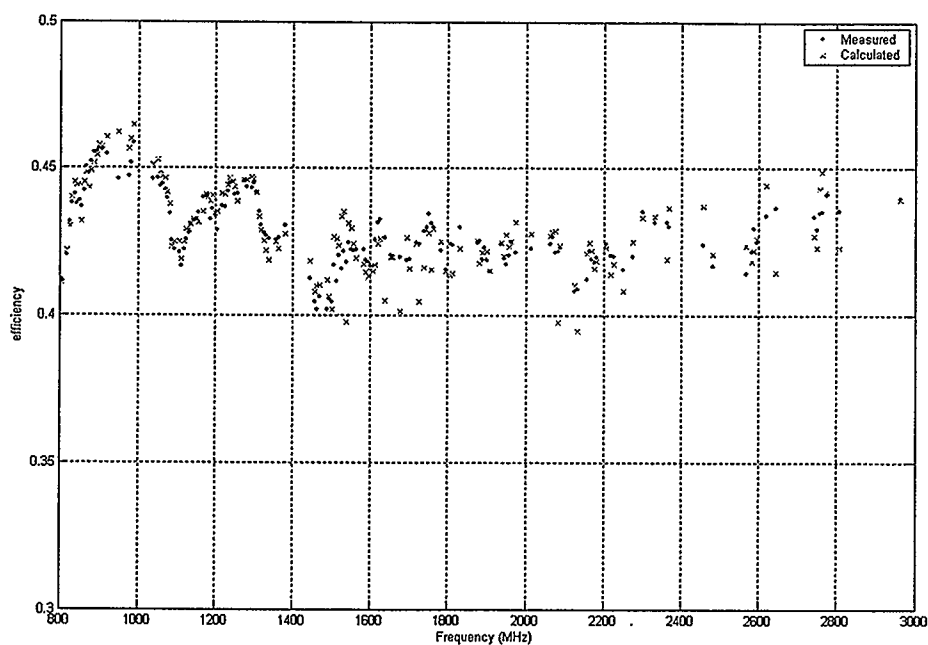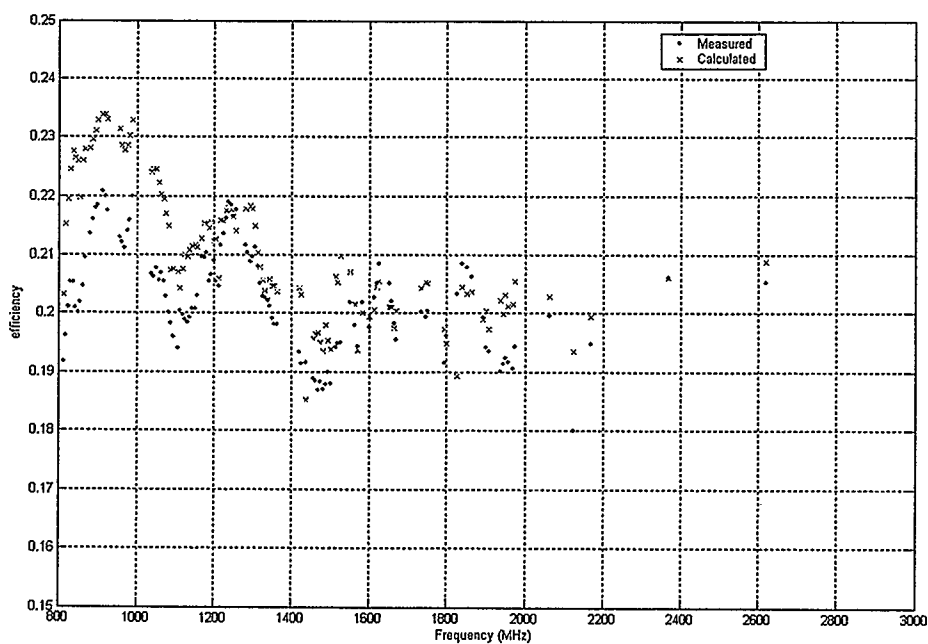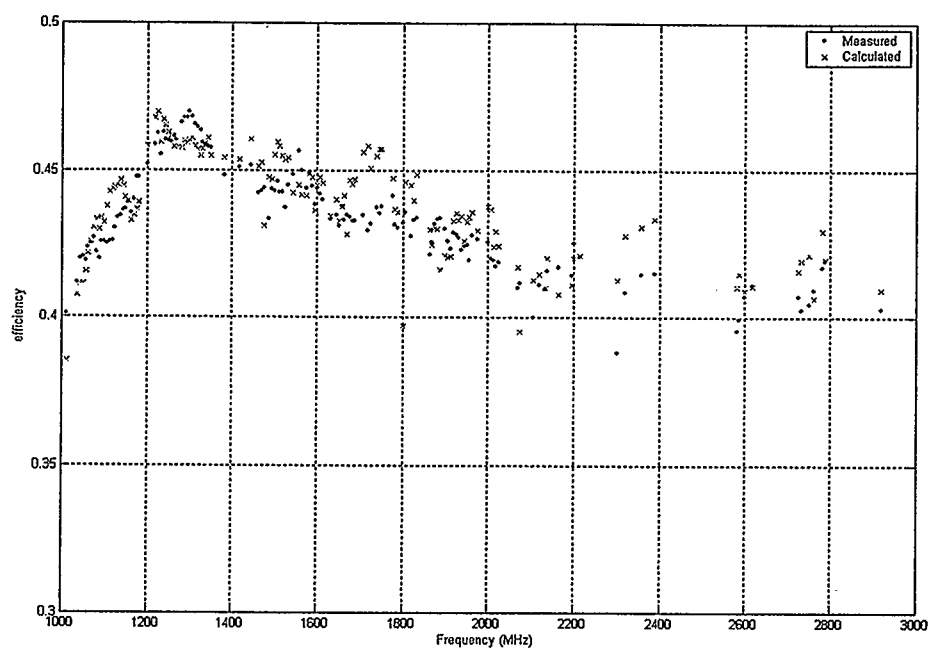
Figure 7.9 The calculated and measured efficiency of the vane antenna #3 with a precision 3dB attenuator with improved data process
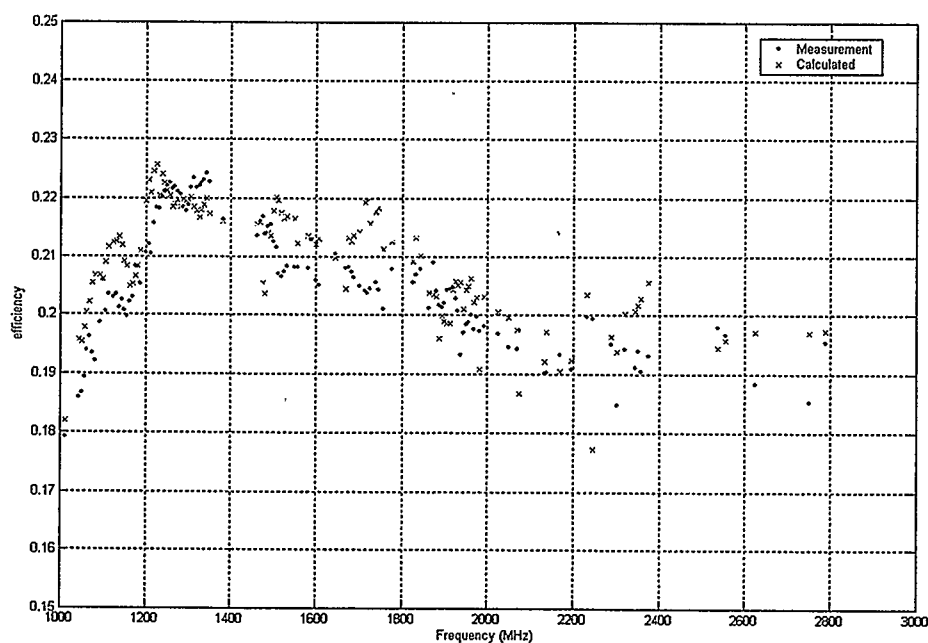

Figure 7.10 The calculated and measured efficiency of the vane antenna #3 with a precision 6dB attenuator with improved data process

Chapter 8

Conclusions

A novel expression for antenna efficiency calculation is treated and measurements are presented. This method removes the assumptions associated with the traditional Wheeler cap method. For example, the traditional Wheeler cap method assumes the antenna's equivalent circuit is a pure series circuit. The presented method can be applied to any electrically small antenna, regardless of its complexity.

A known high efficiency antenna is placed and measured in a rectangular waveguide, a precision rectangular waveguide and in an cubic cavity. The three sets of efficiency measurement are in good agreement with each other in fundamental mode measurement. Efficiency notches occur in multimode measurements. The efficiency notches are attributed to the high losses of higher order modes operating near their cutoff frequency. The precision waveguide is believed to give higher accuracy than the regular waveguide due to its rigid structure and therefore its more consistent cut off frequencies. The cubic cavity gave a better frequency range for accurate measurements than the waveguides. The results of this work indicate that useful efficiency measurements can be carried out in multimode waveguides and cavities but one should be alert to the presence of efficiency notches that can occur due to higher order mode losses at their cut off frequencies.

There are two problems that will affect the accuracy when measuring efficiency over a range of frequency. One is the unevenly distributed S_{11wg} values, another is S_{11wg}

values deviation from the defined circle. Both of them can affect the accurate of circle definition. By applying two criteria, both problems can be reduced substantially although efficiency results are not obtained at all of the measurement frequencies.

References

[1] Warren L. Stutzman and Gary A. Thiele, "Antenna theory and design", John Wiley & Sons Inc., 1998

[2] Constantine A. Balanis, " Antenna theory analysis and design", John Wiley & Sons, Inc., 1997

[3] David M. Pozar and Barry Kaufman, "Comparison of three methods for measurement of printed antenna efficiency", IEEE transaction on antennas and propagation, Vol.36, No1, Jan.1988

[4] Naihong Mao and Xinde Ju, "Antenna Measurement Handbook", National Defense Industry Press (P.R. China), August 1987

[5] Darioush Agahi and William Domino, "Efficiency Measurements of Portable-Handset Antennas Using the Wheeler Cap", Applied Microwave and Wireless, vol. 12, no. 6, pp.34- 42, June 2000

[6] Johnston, R.H., and J.G. McRory, "An Improved Small Antenna Efficiency Measurement Method", IEEE AP-S Magazine, Oct. 1998, pp 40-48

[7] David M.Pozar, "Microwave Engineering", John Wiley & Sons, Inc., 1998

[8] Robert E.Collin, "Foundations for Microwave Engineering", pp.102, McGraw-Hill Book Company, 1966

[9] Yeqin Huang, Narayanan, R.M., Kadambi, G.R., "Antenna-cavity coupling effects on measurement of antenna efficiency", Antennas and Propagation Society International Symposium, 2002, IEEE, Volume: 3, 2002, pp 714-717

[10] Hum, S.V.; Chu, J.; Johnston, R.H.; Okoniewski, M., "Efficiency of a Resistively-Loaded Microstrip Patch Antenna" Antennas and Wireless Propagation Letters, Volume: 2 Issue: 1 , 2003 ,Page(s): 22 -25

[11] H.P.Westman, Ed., "Reference data for radio engineers", Howard W. Sams, 1968

[12] Improving the bandwidth of microstrip patch antennas using resistive loading Hum, S.V.; Chu, J.; Johnston, R.H.; Okoniewski, M., Antennas and Propagation, 2003 IEEE Society International Conference on , Volume: 2 , June 22-27, 2003, Page(s): 276 -279